FABRICATION OF MICROFLUIDIC DEVICES VIA 3D PRINTER

A Thesis Submitted to
The Graduate School of Engineering and Science of
İzmir Institute of Technology
In Partial Fulfillment of the Requirements for the Degree of

MASTER OF SCIENCE

in Biotechnology

by
Seren KEÇİLİ

July 2019
İZMİR

We approve the thesis of **Seren KEÇİLİ**

Examining Committee Members:

Asst. Prof. Dr. Hüseyin Cumhur TEKİN
Department of Bioengineering, İzmir Institute of Technology

Assoc. Prof. Dr. Engin ÖZÇİVİCİ
Department of Bioengineering, İzmir Institute of Technology

Assoc. Prof. Dr. Sinan GÜVEN
Department of Medical Biology, Dokuz Eylül University

17 July 2019

Asst. Prof. Dr. Hüseyin Cumhur TEKİN
Supervisor, Department of Bioengineering
İzmir Institute of Technology

Prof. Dr. Volga BULMUŞ
Co-Supervisor, Department of Bioengineering
İzmir Institute of Technology

Assoc. Prof. Dr. Engin ÖZÇİVİCİ
Head of the Department of Biotechnology and Bioengineering

Prof. Dr. Aysun SOFUOĞLU
Dean of the Graduate School of Engineering and Sciences

ACKNOWLEDGMENTS

Firstly, I would like to express my indebtedness to my advisor Assist. Prof. Dr. H. Cumhur TEKİN for his ideas, suggestions, guidance, support and motivation in all the time of research and writing of this master thesis.

I would like thank to my co-advisor Prof. Dr. Volga BULMUŞ for helpful discussion.

I would like thank to The Scientific and Technological Research Council of Turkey (TÜBİTAK, the grant #116M298) and İzmir Institute of Technology Projects of Scientific Research (BAP, the grant #2017IYTE59) for their financial support during my master studies.

I would like thank to Prof. Dr. Serdar ÖZÇELİK, Prof. Dr. Canan VARLIKLI and Dr. Halide DİKER from Department of Photonic, İzmir Institute of Technology (IZTECH) for their support during spin coating process, Prof. Dr. Metin TANOĞLU, Serkan KANGAL and Zeynep AY from Department of Mechanical Engineering, IZTECH for their support on tensile test and surface contact angle measurements.

I am also thankful the group members of the Laboratory of Biomedical Micro and Nanosystems, IZTECH for helpful discussions and their support throughout my experiments.

I would like thank to Prof. Dr. Kadriye AKGÜN DAR, Department of Biology, İstanbul University and Ahmet AKGÜN for their support all the time.

I warmly thank my dear friends Merve Nur İŞAŞIR, Esra YILMAZ, Funda BİLGİLİ, Hava ZORTAŞ TÜTER and Mert ÜREĞEN. During a stressful and intense master period, they have supported me with their patience and friendships.

I greatly thank my mother Özlem Serpil KEÇİLİ, my father Cavit KEÇİLİ, my brothers Eray KEÇİLİ and Alper KEÇİLİ, my sister Sibel GÜNEL, my grandmothers Türkan KEÇİLİ and Sevgi GÖNCÜ and my grandfather Şakir KEÇİLİ for their moral support, understanding and unconditional love every time.

ABSTRACT

FABRICATION OF MICROFLUIDIC DEVICES VIA 3D PRINTER

The purpose of this thesis is to provide easy and rapid prototyping of microfluidic devices using 3D printing technology that overcomes disadvantages of traditional fabrication techniques and also enhanced optical transparency of 3D-printed microfluidic devices fabricated using new bonding strategies. For performance analysis of 3D printer, microfluidic channels and molds having different shape and dimensions were designed and fabricated. After the fabrication process, designed and fabricated channel dimensions were compared. Structures having at least having 50 μm feature were printed successfully. For enhancing transparency of fabricated 3D structures, two different fabrication techniques were developed. In these techniques, 3D structures were bonded on glass substrates with poly (dimethylsiloxane) (PDMS) and Formlabs Clear Resin interlayers. After 3D-printed structures were put on interlayers coated glass slides, they were either remained on coated slides or transferred on new slides. Bonding between 3D structures and glass slides were provided with UV exposure for resin and with elevated temperature for PDMS interlayers. Bonding strength of fabricated channels was investigated for different thicknesses of PDMS and resin interlayers. The bright-field and fluorescence imaging properties of these channels were also analyzed. Proposed fabrication technique showed 2-fold improved bonding strength and comparable bright-field and fluorescence imaging capability with respect to traditional plasma activated PDMS-glass bonding. Furthermore, protein modified glass substrates can be integrated in 3D-printed channels using the presented fabrication technique without disturbing protein functionality. Finally, in order to design a 3D-printed micropump having membranes that can be activated with compressed air, membrane deformation was characterized with different dimension.

ÖZET

MİKROAKIŞKAN CİHAZLARIN 3B YAZICI KULLANILARAK ÜRETİLMESİ

Bu tez çalışmasının amacı, mikro akışkan cihazların üretiminde kullanılan klasik üretim yöntemlerinin dezavantajlarını ortadan kaldıran 3B yazıcı teknolojisini kullanarak, hızlı ve kolay bir şekilde cihazların prototiplenmesini sağlamak ve yeni yapıştırma yöntemleri kullanarak 3B olarak üretilmiş mikro akışkan cihazların optik olarak şeffaflığını arttırmaktır. 3B yazıcının performans analizini yapmak için, farklı şekil ve ölçülerde mikro akışkan kanallar ve kalıplar tasarlandı ve üretildi. Üretim sonrası, tasarlanan ve üretilen kanal ölçüleri karşılaştırıldı. En az 50 µm ölçüye sahip yapılar başarılı bir şekilde üretildi. Üretilen 3B yapıları optik olarak iyileştirmek için, iki farklı üretim yöntemi geliştirildi. Bu yöntemlerde, 3B yapılar poli(dimetilsiloksan) (PDMS) ve Formlabs Clear Reçine ara katmanlarıyla cam yüzeylere yapıştırıldı. 3B yapılar ara katman kaplı cam yüzey üzerine koyulduktan sonra, ya orada bırakıldı ya da yeni bir cam yüzeye transfer edildi. Cam yüzey ile 3B yapılar arasındaki yapışma, reçine için UV uygulaması, PDMS için ise yükseltilmiş sıcaklık ile sağlandı. PDMS ve reçine ara katmanlarının farklı kalınlıkları için, üretilen kanalların bağlanma kuvveti incelendi. Bu kanalların aydınlık alan ve floresan görüntüleme özellikleri de analiz edildi. Önerilen üretim yöntemi, klasik plazma ile sağlanan PDMS-cam yüzey yapışmasına nazaran iki kat artırılmış bağlanma kuvveti ve karşılaştırılabilir görüntüleme kapasitesi gösterdi. Ayrıca, sunulan üretim yöntemi kullanılarak, 3B yapılar protein ile kaplanmış cam yüzeylerle proteinin fonksiyonelliğini bozmadan birleştirilebildi. Son olarak, 3B yazıyla üretilecek ve basınçlı hava ile aktive olabilecek zar içeren mikro pompa tasarlamak amacıyla, zarların deformasyonu karakterize edildi.

TABLE OF CONTENT

LIST OF FIGURES

Figures **Page**

Figures **Page**

CHAPTER 1

INTRODUCTION

1.1. General Information about Microfluidic Devices

First, microfluidic devices evolved as gas chromatograph in the 1970s[1] and working principle of they based on capillary effects which used to reduce the amount of sample or reagents in chemical analysis[2]. Microfluidic devices are generally defined as transport, well-controlled manipulation, and analysis of micro-level fluids[3-4]. These devices are also known as miniaturized total/ micro total analysis systems (μTASs) and lab-on-a-chip technologies[1, 3]. The micro scale provides several advantages when it compared with macro-scale such as obtain maximum information with low sample and reagent volume, enable using of complicated protocols and provides mimicking of cell microenvironment[3, 5]. Due to supplying multiple function analysis, using of microfluidic devices is became widespread in chemistry, physics, biology including immunoassays, cell analysis, proteomic and metabolomic, drug discovery, pathogen detection and cancer screening, biochemistry, clinical and forensic science, biomedical researches especially in tissue engineering and point-of-care diagnosis[5-7]. In these applications, for doing complex assays such as transport, mixing, separation, labeling, detection in single devices[8-9], microfluidic devices are integrated with microcomponents that are valves, pumps and mixers[10]. Valve and pump are two main components for manipulation and control of fluid in the microfluidic applications[8, 11].

Valves control direction, motion, isolation and separation of fluid[12-14]. They have two types as passive valves containing check and brust valve, and active valves

including pneumatic, electrokinetic and phase change valves[13-14]. While passive check valves provide unidirectional movement of flow, brust valves organize to flow with changing in geometry[14-16]. Active valves depend on energy sources for activation, for instance, electrokinetic valves use electroosmotic flow for the direction of fluid[13]. Phase change valves control flow with volume difference of materials such as wax, hydrogel and paraffin[13-14]. Pneumatic valves usually work with membrane deflection by air pressure[13-14, 17]. According to the working principle, pneumatic valves are classified as normally-open, normally-closed and lifting gate normally-closed valves [18]. In normally-open valves, when pressure is applied to control channel, membrane deforms downward to flow channel and membrane releases after pressure is take away from the channel. Therefore, unidirectional flow provides by the help of membrane deformation in microchannel[19]. Normally-closed valves consist of PDMS based seat in microchannel[20]. For the opening of these valves, a vacuum is applied to membrane and sample flow is provided with membrane deflection[21]. Working principle of lifting gate normally-closed valves is the same with normally-closed valves, but channels and valve seat are fabricated between PDMS layer and solid substrates such as glass and plastic in this type of valve[22].

Pumps provide manipulation[23] and transportation[24] of fluids at small volume and precise flow rate[25] in the system. Pumps are classified as mechanical and non-mechanical pumps[26]. Mechanical pumps, in other words reciprocating displacement pumps [23], are generally used in macro-scale pumps, and they work with actuators which turn electric energy into mechanical work[26]. These type of pumps are categorised such as piezoelectric[23-24, 26], pneumatic[23, 26], thermopneumatic[23-24, 26], electromagnetic[23-24, 26] and electrostatic[26]. Piezoelectric pumps work with deformation of piezoelectric materials such as silicon[27] and ZnO thin film[28]. Pneumatic pumps enable bidirectionally transferring of flow[29] and they are actuated with applying pressurized air to pneumatic valves series[14]. Thermopneumatic pumps base on volume changing of fluid with heating and cooling for providing of flow[27]. Electromagnetic pumps need a magnetic force that indicates magnet or energized coils[27, 30]. Finally, electrostatic pumps work with movement of membrane on oppositely charge plate sides corresponding with Coulomb Law[27]. Non-mechanical pumps that are known also as continuous dynamic flow pumps turn any energy into kinetic energy for generation of flow and they have several types

such as electrohydrodynamic, electroosmotic or electrokinetic, electrochemical and magnetohydrodynamic[14, 18, 23, 26]. While electrohydrodynamic pumps work with electroosmatic force-ions interactions[14], electroosmatic or electrokinetic pumps use electrical double layer-electric field interaction and electrokinetic force[14, 30]. Electrochemical pumps base on generation of gas bubbles which is constituted with water electrolysis[27]. Magnetohydrodynamic pumps use magnetic and electrical field for generation of flow[14].

1.2. Traditional Fabrication of Microfluidic Devices

For fabrication of microfluidic devices, the traditional techniques such as hot embossing, micromachining, and rapid prototyping with soft lithography are used[3, 31-33]. Hot embossing enables transformation from a mold having a pattern of microstructures to polymeric substrates by the help of temperature and pressure force. This fabrication technique consists of four steps that are heating, embossing, cooling and demolding, respectively[34]. Micromachining includes thin film deposition, lithography, etching and substrates bonding steps, and it is classified as hard micromachining that contains separated bulk, surface and high-aspect-ratio micromachining and soft micromachining[35-36].

However, generally, microfluidic devices are fabricated with soft lithography[33]. Soft lithography is a non-photolithographic technique[37] having molding, alignment and bonding steps[7, 32-33]. This fabrication technique includes replica molding, microcontact printing, micromolding in capillaries, microtransfer molding and solvent assistant micromolding[38]. For soft lithography, the pattern is designed by Computer Aided Design (CAD) program and printed on transparent polymer sheet that is used for obtaining a master. The master is used as a stamp or a mold[37]. The poly (dimethylsiloxane) (PDMS) silicone elastomer is commonly used in prototyping of microfluidic devices because this polymer is inexpensive, gas permeable[6], optically clear, biocompatible, flexible [3]. In addition to these, it has low Young's modulus,

resistance to most organic solvents[39], temperature stability, low autofluorescence[40] and electric insulator[41].

The fabrication of microfluidic devices with PDMS replica molding can be summarized in the following. In the clean room, a silicon wafer as a substrate is coated with negative or positive photoresist. After the coating process and alignment of mask with microstructures pattern onto the coated substrate, it is exposed with UV light. At the end of exposure time, the mask is removed from the coated substrate and cured/uncured photoresist is dissolved using developer solutions. Finally, a mold or master having microstructures pattern is fabricated (Figure 1.1.A.). Generally, 10:1 ratio of PDMS is poured onto the mold and it is baked at elevated temperature for curing of PDMS. After curing, channels are obtained by bonding PDMS replica to a substrate such as glass (Figure 1.1.B.).

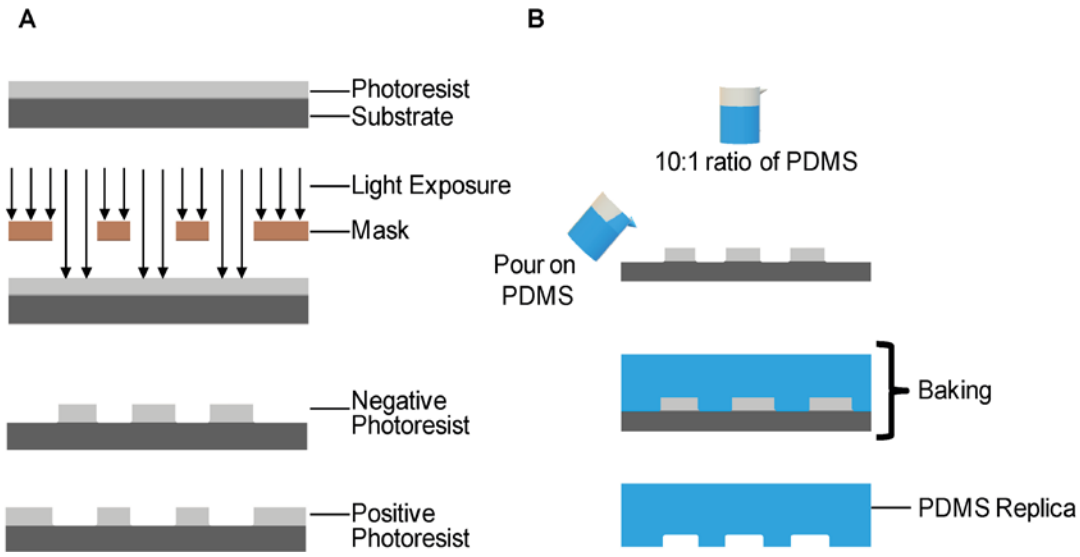

Figure 1.1. Photolithography and soft lithography process for fabrication of microfluidic devices. (A) Shows that photolithography steps (i.e., coating of substrate and light exposure of coated substrates with mask) for fabricating molds with different types of photoresist. (B) Soft lithography process that includes preparation of 10:1 ratio of PDMS and pour on mold, and baking steps to obtain PDMS replica.

However, traditional fabrication techniques have some disadvantages such as the requirement of clean room[41], labour-intensive steps, need of special fabrication tools[3], expensive[40] and slow manual process[42]. Multiple lithography steps and correct layer alignment are essential for the fabrication of three-dimensional (3D) structures. Due to these requirements, the construction of complex 3D structures is challenging[41].

1.3. 3D Printing Technologies

Firstly, 3D printing was developed by Charles Hull in order to fabrication of plastic devices from photopolymer in the early 1980s[43]. 3D printing technologies, which also known as additive manufacturing (AM)[1, 44], rapid prototyping (RP)[43] and solid-freeform technology (SFF)[43], are defined as a single step process[5] that turns a complex 3D digital design into directly physical models[45-46]. In these technologies, 3D structures are designed with a CAD program (AutoCAD, AutoDesk, SolidWorks, Ceno Parametric, etc.) and they are transformed to Standard Tessellation Language or STreoLithography (.STL) file format[47] slicing several 2D cross-sectional parts[48]. Later, 3D structures are fabricated layer-by-layer/point-by-point with different mechanisms[44] from various materials such as plastic, metal or ceramic[49].

3D printing has many different technologies such as stereolithography (SLA)[43, 46, 50], fused deposition modelling (FDM)[48, 51-52], multi-jet modelling (MJM)[44, 50], selective laser sintering (SLS)[43, 48, 52], electron beam melting (EBM)[46, 48, 51], laminated object manufacturing (LOM)[43, 52], photopolymer jetting[46, 52] and binder jetting[46, 52]. In SLA 3D printing technology, the 3D model is produced layer-by-layer from photopolymer[42]/curable resin material[51] exposing laser source or UV light source[46]. SLA technology includes two type technologies which are free surface or bath and constrained surface or bat[46, 53]. In the free surface/bath type, the 3D model is fabricated as 2D cross-sectional parts on the build platform by the laser beam and build platform submerge in the resin reservoir during the 3D printing process. After every fabrication of 2D layer, the build platform is come down by elevator (Figure 1.2.A)[50, 53]. The build platform locates above resin reservoir and 3D model is produced by means of exposing

of the printing material with laser beam from the bottom side of the reservoir in constrained surface or bat type (Figure 1.2.B)[50, 53].

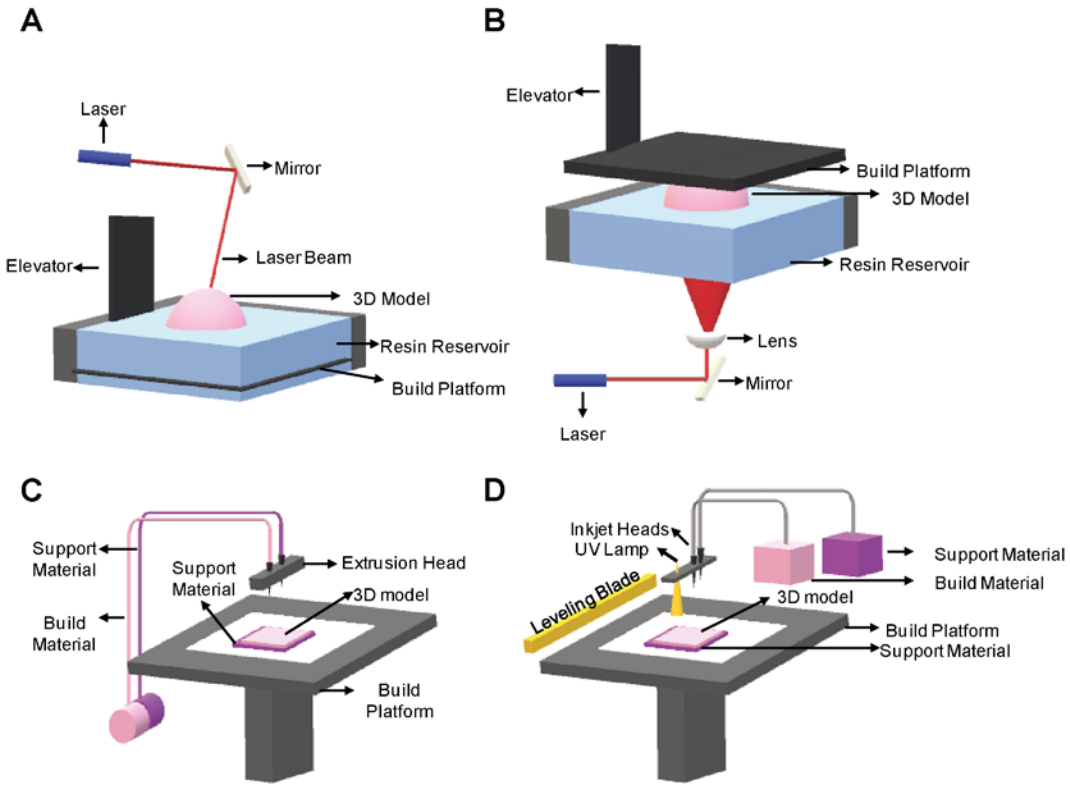

Figure1.2. Illustrations of working principles for different types of 3D printing technologies. Two types of configuration for StereoLithography (SLA) technology (A) bath/free surface and (B) bat/constrained surface configurations. (C) Fused Deposition Modelling (FDM) and (D) Multi Jet Modelling (MJM) technology, respectively.

FDM technology uses thermoplastic filaments as printing material and 3D model is fabricated layer-by-layer on the build platform using thermoplastic materials which are extruded via extrusion head with controlling of temperature (Figure 1.2. C)[43, 53]. In MJM technology, 3D model is produced with UV-curable photopolymer material that is given by inkjet head on the build platform (Figure 1.2.D)[50]. SLS printing technology uses powder as printing material and 3D model is fabricated with heating of powder material which is regulated by a roller in each layer[43, 52]. In EBM technology,

metal powder as a building material is melted by electron beam for fabrication of 3D model[46]. Finally, in LOM technology, material such as paper, plastic and metal located on the building platform and it is cut by laser or razor layer-by-layer[43, 52].

1.4. 3D Printing Technologies in Fabrication of Microfluidic Devices

In recently, using 3D printing technologies becomes widespread in the fabrication of microfluidic devices due to overcoming limitations of traditional fabrication techniques. 3D models having complex geometry[1, 47, 54] are fabricated easily and quickly[41] without specific laboratory experience[55, 56] because of 3D printing technologies. Mainly SLA, FDM and MJM printing technologies use generally for fabrication of microfluidic devices due to their some advantages. SLA technologies provide high resolution during the process when compare with other technologies and reduce printing cost using a trace of photopolymer[43, 51, 53]. FDM is an inexpensive system and different biocompatible building materials can be used such as polycarpolactone (PCL), polylactic acid (PLA) and polyglycolic acid (PGA)[46, 53]. Also, MJM printing technologies enable fabrication of 3D models by more than one material at the same time[50].

SLA technology enables a more effective option for the fabrication of microfluidic devices. Using this technology, either mold for PDMS-based microfluidic devices or directly fabricated microfluidics can be printed[53]. The molds or templates of devices are printed without a mask in a short time[51]. For instance, molds for fabrication of cell lysis microfluidic chamber are printed at nearly 3-5 hr. The replicated two PDMS parts from 3D printed molds are bonded together using corona surface treatment (Figure 1.3.A)[57]. The templates having dimensions from 10 µm to 500 µm are shown to be printed in less than 20 seconds without the requirement of clean room (Figure 1.3.B)[58]. In another work, a master is fabricated with 3D printer for PDMS-based microfluidic devices but due to residual components on 3D-printed master, PDMS is not cured in it. For this reason, post-printed treatments are applied to 3D-printed master. These treatments are heating at 130° for 4 hr, oxygen plasma at high power for 3 min and

coating of 3D-printed master surface using fluorinated silane, respectively. After this treatment process, curing and easily peeling of PDMS is achieved (Figure 1.3.C)[59]. In order to fabricate capillary microfluidic devices using PDMS, a mold is printed. However, after 3D-printed mold surface is treated using a commercial silicone spray, PDMS replica is simply obtained from mold (Figure 1.3.D)[60]. 3D-printed soluble molds having smaller than 200 µm dimension are used to fabricate microfluidic devices and these molds are removed from PDMS solving with organic chemicals after curing (Figure 1.3.E)[61].

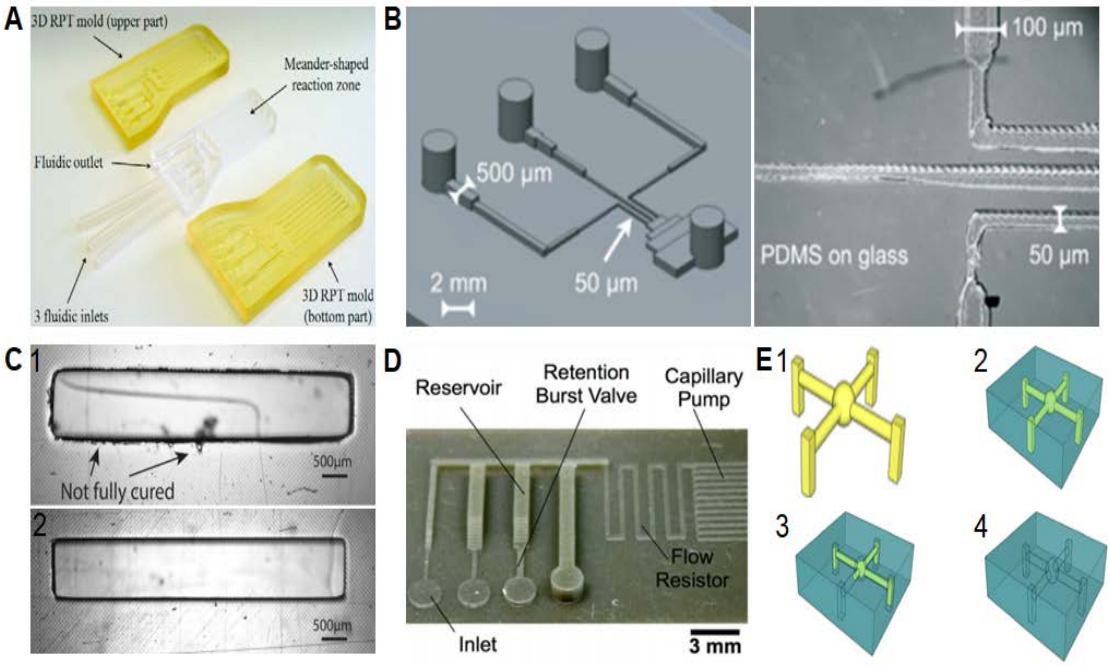

Figure 1.3. 3D-printed molds using SLA technology. (A) Two 3D-printed molds for fabrication of PDMS-based cell lysis chamber (Source: McDonald et al., 2002[57]). (B) 3D CAD design of template and micrograph of PDMS replica (Source: Bonyár et al., 2010[58]). (C) Micrographs for PDMS replica (1) before post-printed treatment process (2) after post-printed treatment of 3D-printed master (Source: Comina et al., 2014[59]). (D) Image of 3D-printed mold for capillary microfluidic devices (Source: Chan et al., 2015[60]). (E) Illustration of fabrication of a PDMS microfluidic device by dissolving mold with chemicals. 3D printed mold (1) in PDMS (2), resolving of mold (3) and final PDMS devices (4) (Source: Olanrewaju et al., 2016[61]).

Microfluidic devices can be integrated with microcomponents such as valve, pump and mixers for complex operation. The devices can be directly fabricated using SLA printing technologies in order to use in many biological and biomedical applications. For instance, a microfluidic device having two channels that their dimensions are 4.3 mm × 1mm (width: height) for cell culture is designed and fabricated with a 3D printer. The bottom surface of this device is coated with a photo resin and they are attached with a semiconductor-based biosensor using UV light exposure for 20 min. In the fabricated microfluidic channel, the activity of cell metabolism is monitored by the sensor. (Figure 1.4.A)[62]. In another work, perfusion cell culture devices with two parts as a top and bottom layer are directly fabricated using a 3D printer. For imaging, the PDMS membrane having 170 µm thickness is put on the glass slide and PDMS membrane/glass slide is placed on the bottom layer. Then, the top layer is attached with the bottom layer using screws (Figure 1.4.B)[63]. In order to detection of pathogenic bacteria, the helical microchannel with 250 µm and 500 µm trapezoidal cross-sectional dimensions is designed and completely fabricated by 3D printer. For the detection, firstly, antibody functionalized magnetic nanoparticles clusters (MNCs) are added to bacteria spiked sample. After free MNCs and complexes of MNCs-bacteria are injected to helical microchannel, MNCs-bacteria complexes are separated magnetically using permanent magnet. Detection limits of 3D printed microfluidic devices are measured as 10 cfu/mL in the buffer and 100 cfu/mL in milk (Figure 1.4.C)[64]. The pump having one inlet, one outlet and three valves is fabricated with a 3D printer using WaterShed XC 11122 as a commercial resin. This 3D printed pump is controlled by a peristaltic sequence with six phases which is 011,001,101,100,110,111 (0: open and 1: closed valve) and pumping rate is calculated ~ 0.68 ml min^{-1} at 75 ms (Figure 1.4. D)[32]. In addition, a pump that includes a valve-like displacement chamber (DC) in between two membrane-based valves (V1 and V2) is completely printed. The 3D printed pump is actuated with air pressure using a sequence with five phases. For V1, DC and V2, the sequence is 000,110,010,011 and 001, respectively and flow rate of the 3D printed pump is measured 40 µL min^{-1} at 15 ms (Figure 1.4.E)[65]. The Quake style pump with flow channel, control channel and membrane that is in between them is designed and fabricated by 3D printer. This pump

is controlled using air pressure with 000,100,011,011,101 operating sequences. Maximum flow rate is measured ~ 6.5 µl min^{-1} at 50 ms (Figure 1.4.F)[66].

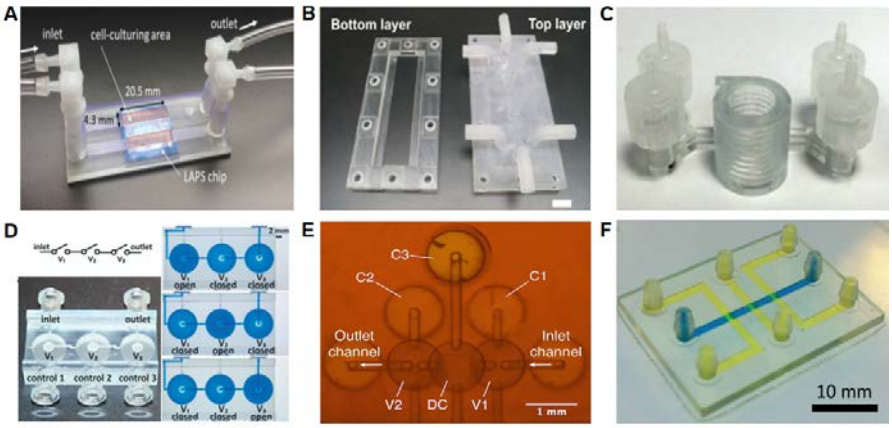

Figure 1.4. Directly 3D-printed microfluidic devices using SLA 3D printer. (A) Sensor-based 3D printed microfluidic channels (Source: Takenaga et al., 2015[62]). (B) 3D printed parts for cell perfusion devices (Scale bar = 1 cm) (Source: Ong et al., 2017[63]). (C) Helical micro channels for detection of pathogenic bacteria (Source: Lee et al., 2015[64]). (D) (Source: Au et al., 2015), (E) (Source: Gong et al., 2016[32]) and (F) (Source: Lee al., 2018[66]) 3D printed pumps having valve systems. The abbreviations in (E) and (F) are as follow; V=valve, C=chamber and DC= displacement chamber.

1.5 Limitations of 3D Printing Technologies

Although 3D printing technologies enable many advantages for microfluidic applications, they have some limitations such as resolution, surface properties, compatibility and transparency[48, 67]. 3D printing technologies are different in terms of used methods and materials and for these reasons, resolution of technologies show difference. For example, microchannels having different dimensions varying between 100 µm-1000 µm width and 50 µm-500 µm height are designed and printed using MJM 3D printer. The designed 100 µm × 100 µm channels resulted in 171 µm × 120 µm (width: height) final dimensions[68]. Using SLA 3D printer, closed channels having

108 µm × 60 µm (width: height) are fabricated successfully[69] and microchannels having 205 µm (±13 µm) dimensions are also printed with FDM 3D printer[70]. Limitation of resolutions causes roughness surface and high dead volume[67]. Surface roughness for FDM and SLA 3D printing technologies is determined as 10.97 µm and 0.35 µm, respectively[70]. 3D printed microfluidic devices are fabricated for biological and biomedical applications. However, the formulation of resins and plastics which are used in 3D printing technologies are not truly known and biocompatibility of materials is important in using applications[50, 67]. For instance, 400 mm^2 × 2 mm circular disks are printed with photopolymer resin. The 3D-printed circular disks are sterilized with UV exposure and 70% ethanol. After sterilization, cells are cultivated on 3D-printed disks. Due to the causing of free radicals on resin with UV exposure, cells had a higher 20% mortality rate than control cells[1].

The materials used in 3D printing process have semi-transparent or non-transparent properties and these properties limit utilization of them for microscopic imaging[67, 71]. The polishing process can physically help to improve the outer surface of 3D printed microfluidic devices but it does not change transparency of the inner wall of channels[67, 72]. 3D printed cell culture and biotest devices are fabricated with MJM and SLA printing technologies but these devices are not optically transparent. For enhanced optical capability, mechanical polishing is applied to out of 3D-printed devices using commercial grit pad and diamond paste[73]. In order to obtain optical transparent microfluidic devices, many different resin formulations are developed. The various mixtures of perfluoropolyether (PFPE) are prepared and the mixtures are optimized for fabrication of transparent and chemically resistance microfluidic devices. Using SLA 3D printer, monolithic channels having 800 µm × 600 µm dimensions (width: height) are fabricated with highly fluorinated perfluoropolyether resin formulation but these devices only are usable to chemical applications (Figure 1.5.A)[74]. Poly (ethylene glycol) (PEG-DA) is biocompatible and photocurable material[75] and for these reasons, resin formulations with PEG-DA are often used in the fabrication of microfluidics. For instance, microfluidic devices having 350 µm × 250 µm channels are printed using resin formulation with PEG-DA but this devices are not suitable for fluorescent imaging and biosensing applications (Figure 1.5.B)[7]. The microfluidic channels are also fabricated with different PEG-DA resin formulation and cell viability is tested with 3D printed

petri dishes. However, due to not gas permeable properties of 3D printed microfluidic channels, utilization of these devices is limited in cell culture and cell imaging applications (Figure 1.5.C)[75]. Besides, microvalve is printed using nearly transparent Watershed XC 11122 as a commercial resin (Figure 1.5.D)[32]. Bottom surfaces of 3D printed microfluidic devices are coated with commercial silicone oil that matched with a refractive index of Watershed XC resin for increasing of optical transparency[42]. Completely transparent microfluidic devices are also fabricated on glass slides with custom made 3D printable PDMS having properties similar to commercial Sylgard 184 PDMS using SLA 3D printer (Figure 1.5.E)[33].

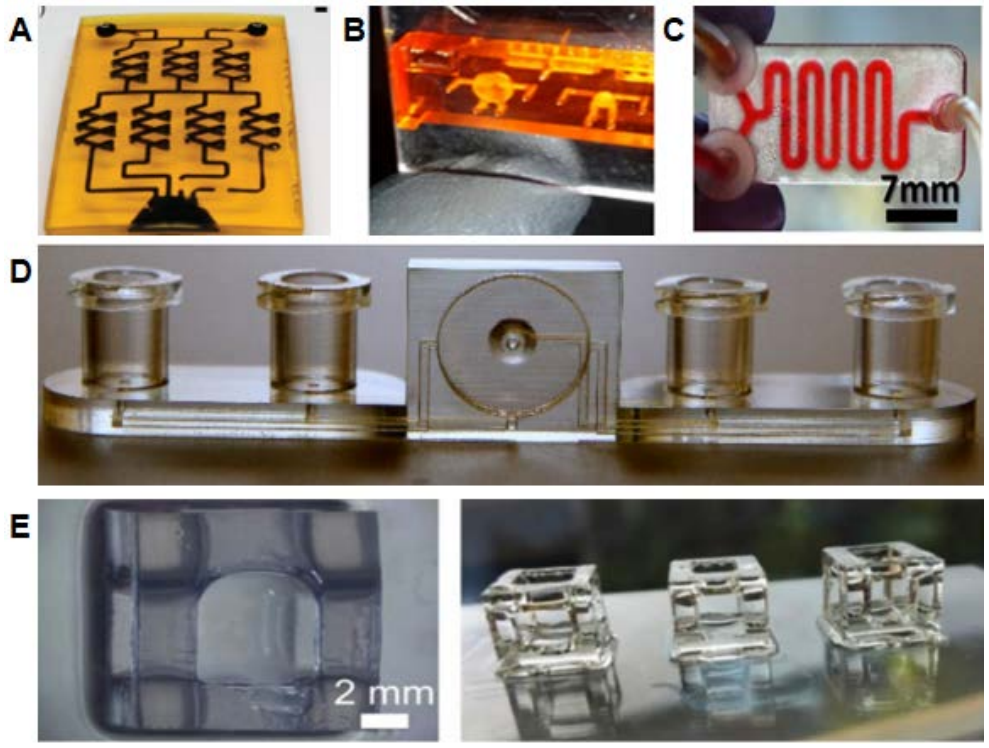

Figure 1.5. 3D-printed microfluidic devices using different resin formulations. (A) Fabricated channels with highly fluorinated perfluoropolyether resin formulation (Source: Kotz et al., 2018[74]). (B) (Source: Rogers et al., 2015[7]) and (C) (Source: Urrios et al., 2016[75]) printed devices using PEG-DA based resin. (D) Fabricated devices with commercial Watershed XC 11122 resin (Source: Au et al., 2015[32]). (E) Printed structures with custom-made PDMS based resin (Source: Bhattacharjee et al., 2018[33]).

Besides, to synthesize of nanoparticles, microfluidic devices are fabricated using poly (lactic acid) (PLA) on the poly (methyl methacrylate) (PMMA) via FDM printing technology. PMMA provides a transparent surface at the bottom of microchannels and nanoparticles inside microchannels are observed under optical microscopy[76]. Pneumatic micromixer is printed using FDM 3D printing technology and Dow Corning 732 as an extrusion material on glass substrate but this silicone material is semi-transparent[77].

3D printed structures are bonded on secondary transparent substrates such as PDMS, glass or polystyrene by heating secondary substrates until above glass transition temperature of commercial 3D printer resin but this process can deform to resin properties [32]. 3D printed microfluidic devices using poly (lactic acid) (PLA) are bonded on PMMA substrates via ethanol as a organic solvent that not change optical transparency property of PMMA under heat and UV exposure, respectively[78]. The microfluidic structures are directly printed on the PDMS, poly (ethylene terephthalate) (PET) and poly (ethylene naphthalate) (PEN) substrates that are treated with silanization as a surface-functionalization. The presented microfluidic devices resisted up to 1.1 bar pressure[79]. Silanization is used for bonding epoxy-based resin to PDMS at room temperature and bonding strength of the prepared samples is 3.5 bar[80]. 3D printed microfluidic channels are also bonded on the flexible structures using UV curable ink that withstands until 1 bar pressure[81].

1.6. Protein Measurements on 3D-Printed Microfluidic Devices

Bioanalysis in microfluidic devices allows high sensitivity, rapid and low-cost analysis with a minute sample consumption[82]. Especially, sensitive protein detection is important in medical and biological applications in terms of early detection and diagnosis[83-84]. For these applications, using 3D printing technologies, in the fabrication of optically enhanced microfluidic devices ensures automation, low cost and processing at short time[82]. For instance, in order to multiple detections of protein biomarkers, a 3D immunoarray device having 40 mm × 35 mm × 3.5 mm (length: width: height) is

fabricated by Formlabs Form 2 SLA 3D printer and this device is coated with acrylic spray for enhancing optical clarity. The open detection chamber of the 3D-printed chip is bonded on a pyrolytic graphite sheet using adhesive. The sandwich immunoassay is made on a single-walled carbon nanotube forest (SWCNT) in micro chip. For immunoassay, Ru $(bpy)_3^{2+}$-silica nanoparticles (RuBPY-SiNP) are coated with detection antibodies (Ab_2) and capture antibodies (Ab_1) are attached on SWCNT forest. Then, the samples and reagents are given into chambers of the 3D-printed chip by micropump and protein biomarkers are detected using electrochemiluminescent (ECL) methods with CCD camera in 25 minutes (LOD is 85-110 fg/mL^{-1}) (Figure 1.6.A.)[85].

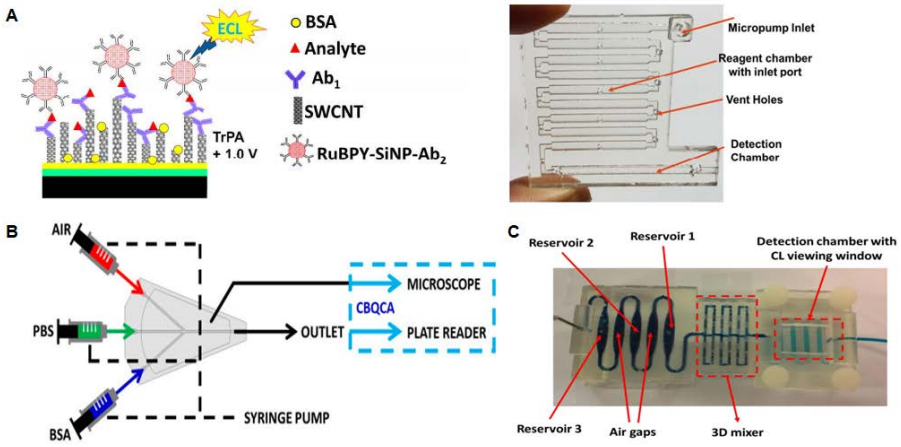

Figure 1.6. 3D-printed microfluidic devices for protein measurements. (A) Illustration of sandwich immunoassay and image of 3D-printed microarray chip. Tripropylamine (TrPA) and RuBPY-SiNP with Ab_2 are used for ECL detection (Source: Kadimisetty et al., 2018[85]). (B) 3D-printed chip and determination of protein. The protein level in the outlet sample is analyzed with CBQCA kit using a microscope and plate reader (Source: Lepowsky et al., 2018[86]). (C) Image of 3D-printed immunoarray device (Source: Tang et al., 2017[87]).

Using FDM 3D printer with PLA, microfluidic devices are directly printed on PMMA substrates that are supply optical transparency. The total protein concentration is monitoring clearly in 3D-printed channels using Bradford method that is a

colorimetric analysis. The protein concentration is calculated successfully until 7.5 mg L^{-1} in 3D-printed channels[88]. The 3D microfluidic chips having three inlets for sample, solution and air are fabricated with Formlabs Form 2 SLA 3D printer. The outside of 3D-printed devices is coated with PDMS for optical clarity. Bovine serum albumin (BSA) as protein, phosphate buffered saline (PBS) as washing solution and air are injected to inlets using syringe pump. The protein level throughout channels is determined using 3-(4-carboxybenzoyl) quinoline-2-carboxaldehyde (CBQCA) protein quantitation kit which is excited with blue light at the presence of protein according to fluorescent light intensity (Figure 1.6.B.)[86].Besides, cancer biomarker proteins are detected with a chemiluminescence method using 3D-printed immunoarray devices with detection chamber and mixer at 30 minutes. In this method, capture antibodies are immobilized on poly-L-lysine coated glass slide at 4°C for overnight. Phosphate buffer saline (PBS) for washing and casein for blocking of non-specific binding are used. The solution of detection antibodies and reagent are given to reservoirs on 3D-printed device and controlling of flow through channels is provided with syringe pump. Chemiluminescence (CL) reagent is injected to detection chamber and CL is measured with bioimaging systems (Figure 1.6.C.)[87].

The purposes of this master thesis are overcome limitations of traditional fabrication techniques for microfluidic devices using SLA 3D printing technology and enhance optical transparency of 3D-printed structures with new hybrid fabrication techniques. Firstly, characterization and performance analysis of Formlabs Form 2 Desktop SLA 3D printer were investigated. To do so, channels and molds having various dimensions and shapes were printed and images of them were analyzed. Secondly, 3D-printed structures were bonded on glass substrates with PDMS and Formlabs Clear Resin FLGPCL02 using different bonding techniques. For bonding process, thickness values of PDMS and resin were determined at different spinning speed and material properties of resin were analyzed. In the direct bonding techniques, 3D-printed structures were directly placed on PDMS or resin interlayer coated glass slides. For the transfer bonding technique, 3D-printed structures were put on new glass slides after they were immersed on interlayer coated glass slides. The heat and UV light were used for curing of PDMS and resin interlayer, respectively. In order to characterization of bonded 3D-printed structures using different interlayer thickness,

bonding strength test was applied to them using air pressure. Optical properties of bonded 3D-printed microfluidic channels for bright-field and fluorescence microscopy imaging were also analyzed and compared with traditional bonded PDMS/glass using plasma. Moreover, 3D printed microfluidic channels were integrated with protein-modified surfaces for biosensing applications using the presented bonding technique. Finally, micropump systems were integrated with microfluidic channels. To do so, theoretical membrane deformation values were calculated and different designs were fabricated by SLA 3D printer. The micropump was bonded on glass slides using presented bonding technique. The characterization analysis of micropump was made using valves for controlling.

CHAPTER 2

MATERIAL AND METHODS

2.1. Materials

2.1.1. Consumables

Glass slides (Marienfeld, Germany) were used as bonding substrates. For all test with microfluidic structures, the connection between 3D structures and air supply was provided with Tygon® tubing (Tygon® Saint-Gobain, U.S.A). The leakages and other observations in channels were tested using Red Food Dye (Ozmen Food Products, Turkey). N_2 gases (Gunes Gas, Turkey) was used for pressure supply. In order to the fabrication of channels using soft lithography, Poly (dimethylsiloxane) (PDMS) (Sylgard 184, Sigma-Aldrich, Germany) was used. Needles having 1.4 mm inner diameter (C3 Technology, Turkey) were used to make holes in PDMS chip. Formlabs Clear Resin (FLGPCL02, Formlabs, USA) was selected for 3D printing and bonding process. Pattex Power Epoxy (Pattex, Australia) was used for attachment of tubing with 3D structures. In fluorescent imaging tests, 10-20 μm Red and Green Microspheres (Cospheric LLC, CA) were used. Tween®20 (Sigma-Aldrich, Germany) was used for the preparation of microsphere solution.

Isopropanol (VWR International, U.S.A) for removing of uncurable printer resin and ethanol (Merck, Germany) to clean glass slides were used. In order to make surface modification, (3-mercaptopropyl) trimethoxysilane (3-MPS) (Sigma-Aldrich, Germany) solution was prepared in 200 Proof Ethanol (K50322183 825, Merck, Germany). In protein immobilization, N-γ-maleimidobutyryl-oxysuccinimide (GMBS) (Thermo

Fisher Scientific, USA) as cross-linker, Phosphate Buffered Saline (PBS) (Thermo Fisher Scientific, USA) for washing, Bovine Serum Albumin (BSA) (Sigma-Aldrich, Germany) for blocking were used. Dimethyl sulfoxide (DMSO) (Sigma-Aldrich, Germany) was used for the preparation of GMBS stock solution. Protein patterning was made using Pierce® Recombinant Protein G (Thermo Fisher Scientific, USA) spiked in PBS. Pluronic® F-127 (Sigma-Aldrich, Germany) was used for washing and Goat Anti-Mouse IgG (H+L) Antibody Labeled with Alexa Fluor™ Plus 488 (Thermo Fisher Scientific, USA) in Pluronic® to test Protein G patterns was used.

2.1.2. Equipment and Softwares

For fabrication of 3D structures, Formlabs Form 2 Desktop-SLA 3D printer (Formlabs, USA) was used. All microscopic observation was made under Zeiss Axio Vert A1 inverted fluorescent microscope (ZEISS, Switzerland) having Colibri 7 Type RGB-UV LED illumination (385/30 nm, 469/38nm, 555/30 nm and 631/33 nm excitation bandwidths) and Zeiss filter set FS 90 HE. Oxygen plasma (ZEPTO, Diener, Germany) was used for surface treatment. During the coating process, Laurell WS-400B-6NPP/LITE spin coater (Laurell Technologies Company, U.S.A) was used. Attension Theta tensiometer (Biolin Scientific, Sweden) for surface contact angle and Shimadzu AGS-J 5kN tensile test device (Shimadzu, U.S.A) in classical tensile stress test were used. Micropump was controlled using Festo solenoid valves (FESTO, Germany) and Arduino Uno (Arduino, Italy). Ultrasonic bath (Isolab, Germany) was used in order to the cleaning of glass slides. Incubator (Memmert, Germany) and UV box having 370 nm and 36 W (JD-818, Yani Minicure Supplies Company, China) were used to the curing of PDMS and printer clear resin, respectively.

Through studies, AutoCAD (Student Version, Autodesk Inventor, California) for 3D designing and Preform (https://formlabs.com/software/) (Formlabs, USA) as 3D printer slicer program and ImageJ to analyze images were used.

2.2. Methods

2.2.1. The Fabrication of Microfluidic Structures via 3D Printer

The 3D structures having intended shapes and dimensions were designed by the help of AutoCAD software (Figure 2.1.A). The designed 3D structures were tilted 30° and supports were added to each structure using Preform software as a printer slicer program. This program slices 3D structures to 2D cross-sectional parts for layer-by-layer fabrication on 3D printer (Figure 2.1.B). 3D structures, which were made suitable for 3D printer, were fabricated with UV curable Formlabs Clear Resin using Formlabs Form 2 desktop stereolithography 3D printer at high resolution (Figure 2.1.C). At the end of the printing process, all 3D structures were washed with isopropanol twice for 10 minutes for removing of uncurable resin and support on 3D structures was cleaned.

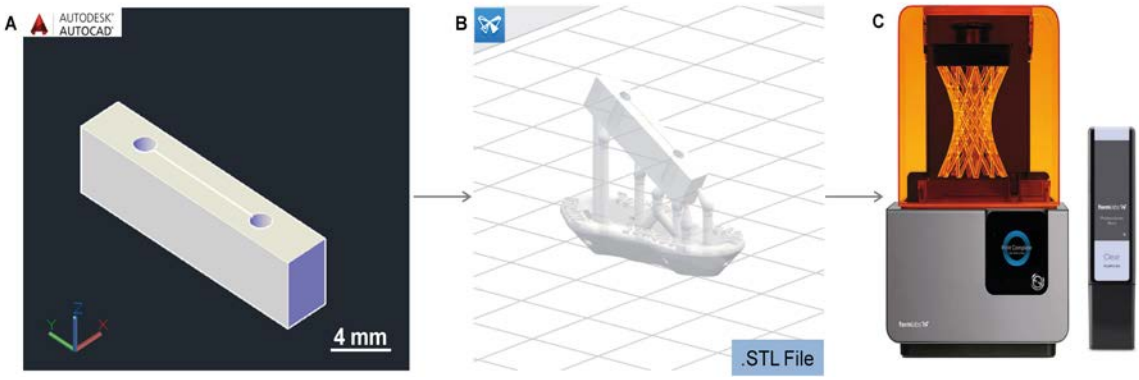

Figure 2.1. Design and fabrication of 3D structure using Formlabs Form 2 SLA 3D printer and process steps. (A) CAD design of 3D structures and file format is turned into.STL file. (B) Doing necessary editing for 3D structures via slicer program. (C) Printing of 3D structures by SLA 3D printer using UV-curable resin.

2.2.1.1. Performance Analysis of 3D Printer

In order to characterization of 3D printer, semi-circular open channels, rectangular open channels and their correspondingly molds with 2:1 aspect ratio (width: height) having 50 µm, 75 µm, 100 µm, 125 µm, 150 µm, 175 µm, 200 µm, 225 µm and 250 µm height dimensions were designed (Figure 2.2.A-B). Besides, closed square channels with 500 µm, 600 µm, 700 µm, 800 µm, 900 µm and 1000 µm dimensions were also designed (Figure 2.2.C.). These channels and molds were fabricated with SLA 3D printer. After the printing process, 3D printed closed channels, open channels and their corresponding molds were observed under Zeiss Axio Vert A1 inverted fluorescent microscope. The fabricated dimensions were analyzed with ImageJ software and they were compared with designed dimensions.

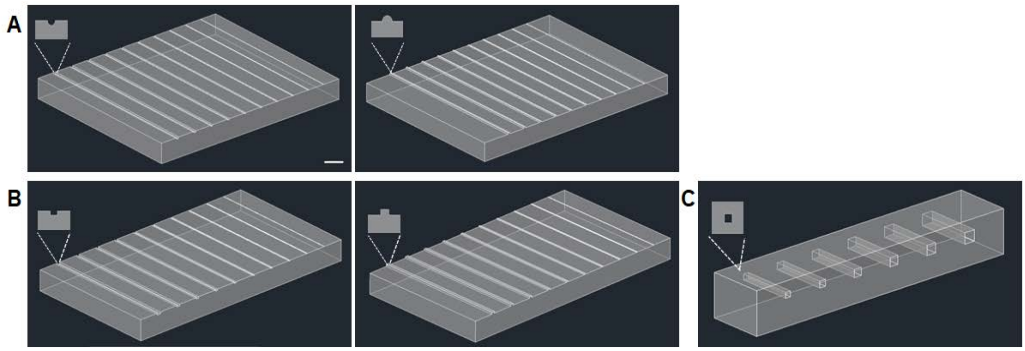

Figure 2.2. CAD design and cross-sectional views for channels and molds. (A) Semi-circular open channel and its molds, (B) rectangular open channel and its mold and (C) closed square channel. Scale bar is 3 mm.

2.2.2. Bonding of 3D Printed Structures on a Glass Substrate

Two bonding strategies were used for attachment of 3D-printed structures to glass substrates with PDMS and resin as bonding materials. The glass substrates were

cleaned with 70% ethanol for 10 min using the ultrasonic bath. To preparation of PDMS, elastomer and curing agent were mixed at 10 to 1 ratio. The vacuum was applied to mixed PDMS until all the bubble disappears from it. Before coating process, prepared PDMS was waited for 1 hr at room temperature. The cleaned glass substrates were treated with 100W air plasma at 0.5 mbar for 2 min using ZEPTO oxygen plasma for only PDMS spin coating. Liquid PDMS and resin were coated on glass substrates using Laurell spin coater at 1000 rpm, 2000 rpm, 3000 rpm and 4000 rpm spinning speeds for 30 s (at 500 rpm for 10 s and at the final spin rate for 20s) (Figure 2.3.A.). Each spinning rate was resulted in different coating thickness. In the first bonding technique, which is direct bonding technique (Figure 2.3.B), 3D-printed structures were directly put on the interlayer coated glass substrates. However, in transfer bonding technique (Figure 2.3.C), 3D-printed structures were transferred to cleaned glass substrates after 3D-printed structures were put on interlayer coated glass substrates. The bonded 3D-printed structures using PDMS were cured at 80°C for 12 hr in the incubator. The UV exposure at a wavelength of 370 nm using 36 W UV box was applied to resin interlayer for 10s. After the curing process, bonding of 3D-printed structures on the glass substrates was achieved.

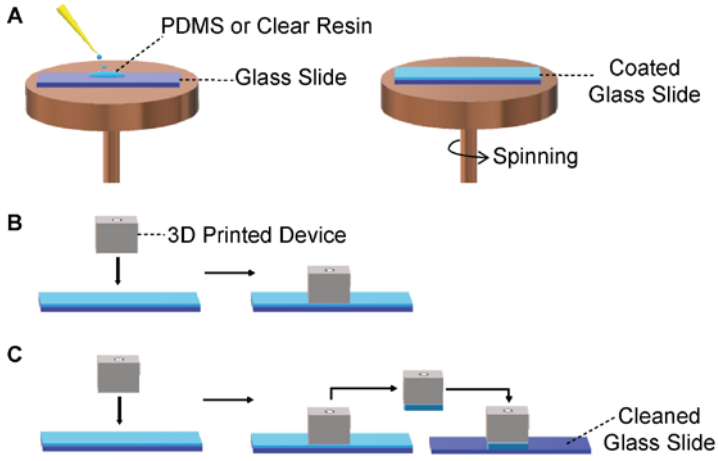

Figure 2.3. Illustration of bonding techniques and cross-sectional views of 3D-printed devices after the bonding process. (A) Coating of the cleaned glass substrate with PDMS or resin. (B) Direct bonding technique and (C) Transfer bonding technique.

2.2.2.1. Characterization of Bonded 3D Printed Structures

For bonding strength test, cylindrical chambers having 2.5 mm radius, 1 mm height and 1.4 mm single inlet on top within a square block having 15 × 15 × 4 mm dimensions and their correspondingly mold were designed and fabricated (Figure 2.4.A-B). 3D-printed chambers were bonded on a glass slide with PDMS and resin interlayer using direct and transfer bonding techniques. For replica molding with PDMS, 10:1 ratio of PDMS was pour into the 3D-printed mold and cured at 80°C for 12 hr. After curing, inlet was opened via needle having 1.4 mm inner diameter and PDMS chambers (Figure 2.4.B.) were bonded to glass slides, which were previously cleaned using 70% ethanol, by treating of bonding surfaces with 100W air plasma at 0.5 mbar for 2 min using oxygen plasma. Tubing having 1.5 mm diameter was attached to both 3D-printed chamber and PDMS chamber by epoxy. Red food dye was injected to tubing and air pressure from 1 bar to 10 bar with 0.5 bar incremental steps was applied to prepared samples for 2 min for each pressure values using compressed air supply (Figure 2.4.C.). Leakages were inspected under an inverted fluorescent microscope.

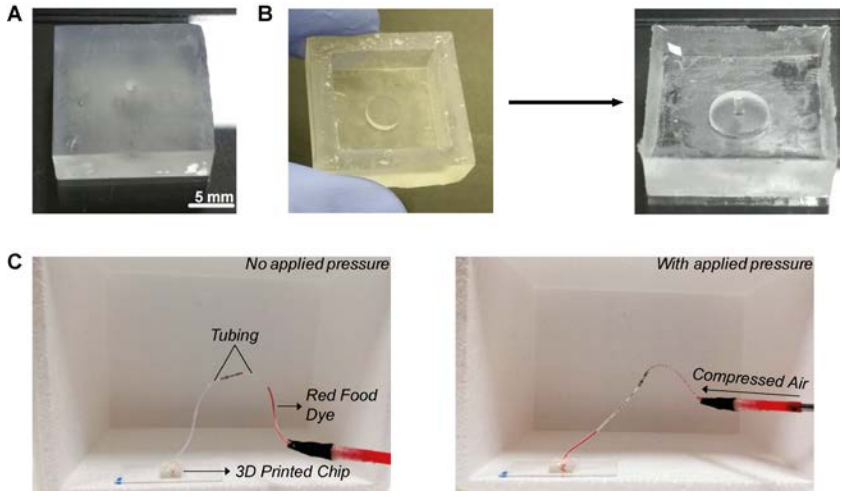

Figure 2.4. Bonding strength test chambers and test process. (A) Photographs of the 3D-printed test chamber, (B) its 3D-printed mold and PDMS replica test chamber. (C) Bonding strength test process before and after applied pressure.

For tensile stress test, glass slide was cleaned with 70% ethanol and coated with resin at 1000 rpm. 3D printed chamber was bonded on glass slide using transfer bonding technique and UV light was applied for 10 s. The supports were added to the prepared sample with epoxy and test was made by Shimadzu AGS-J 5kN test device (Figure 2.5.).

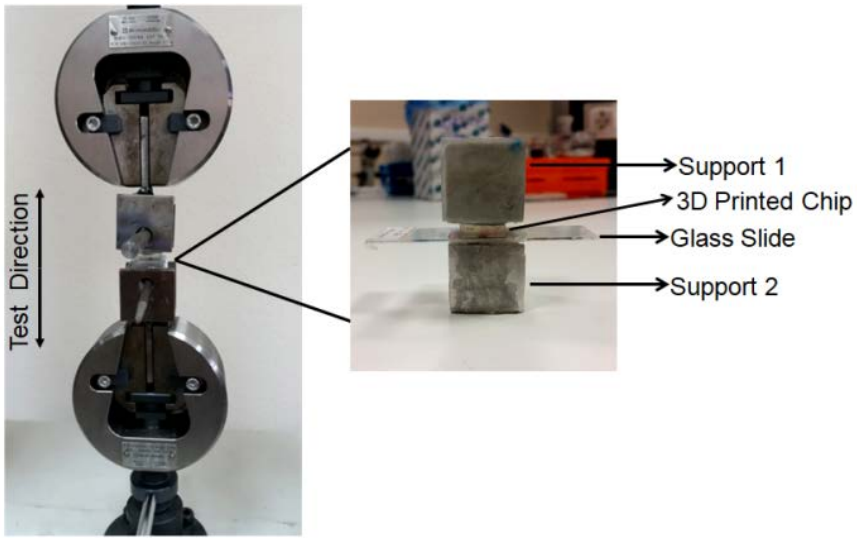

Figure 2.5. Tensile stress test for fabricated chip using transfer bonding technique.

Surface contact angle measurements were also made using tensiometer. For this, square block having 25 mm × 25 mm × 1 mm dimensions was designed and fabricated with SLA 3D printer. After glass slide that cleaned with 70% ethanol was treated with O_2 plasma, it was coated with 10:1 ratio of PDMS at 1000 rpm and cured at 80°C for 12 hr, respectively. Finally, the surface contact angle of glass slide, prepared PDMS substrate and square block were measured before and after O_2 plasma treatment.

Time-dependent accumulation of resin on the glass slide was analyzed. To do so, glass slide was cleaned with %70 ethanol for 10 min by the ultrasonic bath. Later, glass slide was coated with resin at 1000 rpm and images of coated glass slide were taken for 10 min.

Before and after applied bonding techniques, heights of channels were analyzed. To do so, 400 µm × 400 µm cross-sectional open-ended channels were designed and fabricated with 3D printer. Before the bonding process, the height of channels was measured from micrographs. The channels were bonded on glass slide with PDMS and resin using direct and transfer bonding technique at 1000 rpm, 2000 rpm and 3000 rpm. After the bonding process, red food dye was injected to the microchannels and they were inspected under a microscope with 5× objective. Finally, the height of channels before and after the bonding process was compared.

In order to test microscopic imaging capability of fabricated channels using bonding techniques, open-ended square channels with 400 µm × 400 µm dimensions were used. Molds having 400 µm × 400 µm square channel were designed and fabricated to compare traditional PDMS/glass chip with 3D-printed chip. Fluorescent red and green microspheres were prepared in 2% (v/v) PBS-Tween solution and the prepared solution was injected to microchannels. After injection, microchannels were imaged under fluorescent microscope with 20× objective. Image analysis of captured micrographs was made using ImageJ. The fluorescence intensity value of red and green fluorescence microspheres was measured using equation (2.1).

$$FI = Mean\ fluorescence\ of\ microspheres - Mean\ fluorescence\ of\ background \quad (2.1)$$

2.2.3. Protein Immobilization and Characterization

2.2.3.1. Design of Microfluidic Channels

A 3D-printed mold having 1 mm × 1mm three vertical channels for Protein G patterning (Figure 2.6.A), 3D-printed chip having 1 mm × 1mm dimensions and corresponding mold for selective IgG binding (Figure 2.6.B) were designed and

fabricated using 3D printer. In order to attachment of PDMS chips to glass slides, external plates having six holes at 4 mm diameter for screwing, three inlets and three outlets with 3 mm diameter for each one were also designed and fabricated by 3D printer.

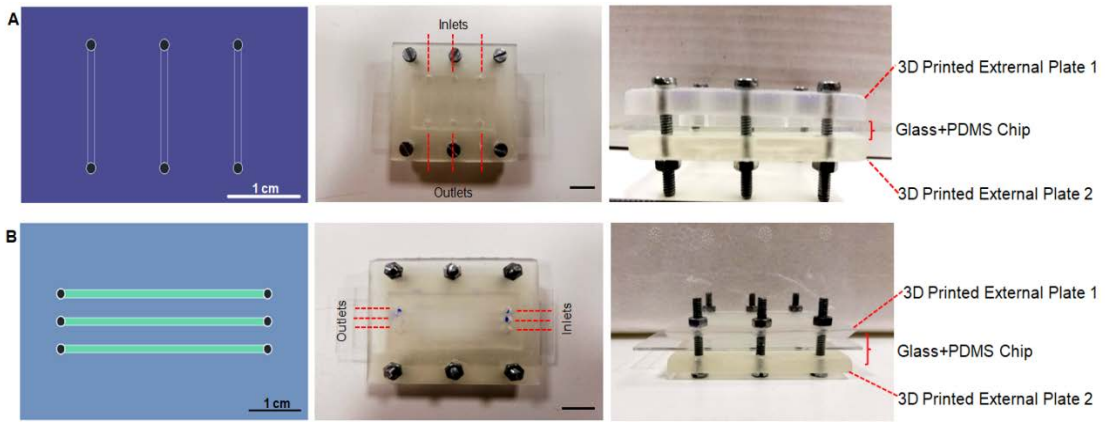

Figure 2.6. Microfluidic channels for protein immobilization. (A) Protein G and (B) IgG binding channels. Top and side views of attached PDMS chips on glass slide via external plates were shown. Scale bars are 1 cm.

2.2.3.2. Protein Immobilization

10:1 ratio of PDMS was prepared and poured on the molds for PDMS chips and the molds were incubated at 80°C for 12 hr. Glass slides were cleaned with 70% ethanol using ultrasonic bath for 10 min, dried with N_2 gas and treated with 100W air plasma at 0.5 mbar for 2 min, respectively. For the preparation of 4% (v/v) 3-MPS solution in 200 proof ethanol, 600 µL stock 3-MPS solution and 15 mL 200 proof ethanol was mixed. The cleaned glass slides were incubated in 4% (v/v) 3-MPS solution for 45 minutes at dark environment. After silanization, the glass slide was rinsed with 1mL 200 proof ethanol and dried at room temperature. The dried glass slide was sealed with PDMS chip via external plates for protein patterning. For GMBS stock, 50 mg GMBS was

diluted with 250 µL DMSO and 1.2 mg/mL GMBS solution was prepared mixing 3 µL GMBS stock and 500 µL PBS. After sealing, channels were washed with PBS two times, 1.2 mg/mL GMBS solution was given to channels and incubated for 45 minutes in a dark environment at room temperature. 10 µL Protein-G stock was prepared with diluting of 5 mg Protein-G in 1000 µL PBS. 240 µL PBS and 10 µL Protein-G stock was mixed for preparation of 0.2 mg/mL Protein-G solution. The channels are cleaned with PBS and then, 0.2 mg/mL Protein-G solution was injected to channels and incubated for overnight at 4°C (Figure 2.7.A). After Protein-G immobilization, channels were washed with PBS, dried using N_2 and PDMS chip was removed from the glass slide. For bonding of 3D-printed chip to glass slide having immobilized Protein-G, transfer bonding technique was used with spin-coated resin at 1000 rpm. The PDMS chip was also attached to the glass slide using external plates. For preparation of 1% (w/v) BSA solution, 0.05 g lyophilized BSA was diluted in 5 mL PBS and this solution was injected to channels and incubated for 30 minutes at 4°C. 1% (w/v) Pluronic solution was prepared with mixing of 1 g Pluronic stock and 100 mL PBS and this solution was diluted ratio of 0.1%. The channels were washed with 0.1% (w/v) Pluronic solution prepared in PBS, and then 50 µg/mL goat anti-mouse IgG (H+L) antibody solution prepared in 0.1% Pluronic (3 µL antibody + 117 µL 0.1% Pluronic) was given in the channels and incubated for 30 min at 4°C (Figure 2.7.B). Before inspection under microscope, the channels were cleaned with 0.1% Pluronic solution three times and after washing, prepared samples were inspected under fluorescent microscope using 5 × objectives. Furthermore, unspecific Ab absorption and autofluorescence issues of the presented protocol were tested in PDMS channels. For unspecific Ab absorption test, glass slide was patterned with BSA instead of Protein-G and other protocol steps were kept the same. For autofluorescence test, Protein-G was also immobilized on glass slide using the presented protocol but Ab solution was not injected to channels. At the end of these processes, samples were observed under fluorescence microscope with 5× objective. Micrographs of all prepared samples were analyzed using ImageJ software. Fluorescence intensity of the prepared sample was calculated with equation (2.2).

$$FI = Mean\ fluorescence\ of\ protein\ pattern - Mean\ fluorescence\ of\ background \quad (2.2)$$

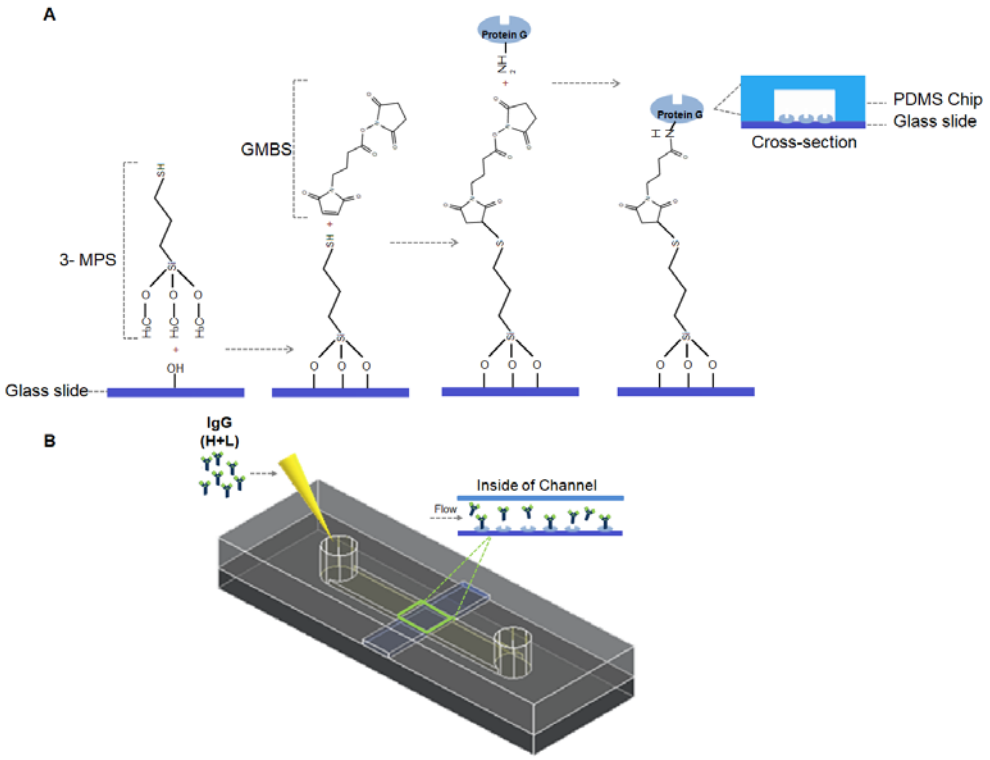

Figure 2.7. Protein-G immobilization and selective IgG (H+L) binding process. (A) Protein-G immobilization using GMBS cross-linker on the silanized glass slide. (B) Illustration of selective IgG (H+L) binding on Protein-G patterns inside the channel. The chemical structures were drawn using ChemSpider online program (Royal Society of Chemistry).

2.2.4. Micropump

2.2.4.1. Theoretically Membrane Deflection Measurements

For membrane-based micropump designing, membrane deformations were measured by equation (2.3)[32]. The equation includes some factors, which are pressure (*P*), Young's modulus of material (*E*), necessary membrane radius to close the gap (*r*),

predict membrane deflection (y), membrane thickness (t) and Poisson's ratio of material (v).

$$\frac{Pr^4}{Et^4} = \frac{5.33}{1-v^2} \cdot \frac{y}{t} + \frac{2.6}{1-v^2} \cdot \left(\frac{y}{t}\right)^3 \qquad (2.3)$$

For two membrane deformation model, membrane deformations were calculated. First model having t = 250 µm, y = 250 µm and r = 5000 µm and second model with t = 500 µm, y = 250 µm and r = 7500 µm. were designed (Figure 2.8.) and completely fabricated by 3D printer. The Young's modulus and Poisson's ratio of resin are 2800 MPa and 0.5, respectively. According to equation 2.3, predicted deformation pressure of membrane was measured 1.85 bar and 2.05 bar for the first model and second model, respectively. The inlets of 3D-printed deformation devices were integrated with tubing for applying air pressure and outlets of them were closed using epoxy. 2 bar, 4 bar, 6 bar and 8 bar air pressure were applied for 2 min each pressure value. The membrane deformation was inspected under microscope and deformation height was measured using ImageJ.

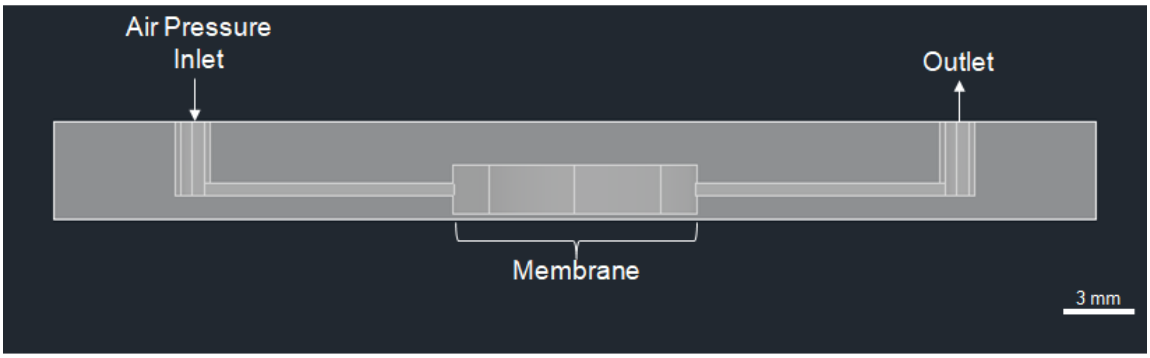

Figure 2.8. CAD design of used models for membrane deformation.

2.2.4.2. Design and Fabrication of Micropump

A micropump design includes three valves that compose of three control channels (C1, C2, C3), three fluid channels (F1, F2, F3), three membranes (M1, M2, M3) in between control and fluid channels and two via (V1, V2) that provide connection between fluidic channels. The control channels involve a chamber having 5000 µm radius and 700 µm height, two channels with 2000 µm × 700 µm (width: height), an inlet and an outlet having 700 µm radius. The first and third fluid channels consist of a chamber with 5000 µm radius and 700 µm height, one channel (on left or right) having 2000 µm × 700 µm (width: height) and via having 1000 µm radius at the center of the chamber. The different from these channels, chamber height of the second fluid channel is 2000 µm and this channel have two channels with 2000 µm × 700 µm (width: height). The second fluid channel connects with first and third fluid channels using two via and bottom of this channel was left open. The thickness of membranes is 250 µm (Figure 2.9.A.).

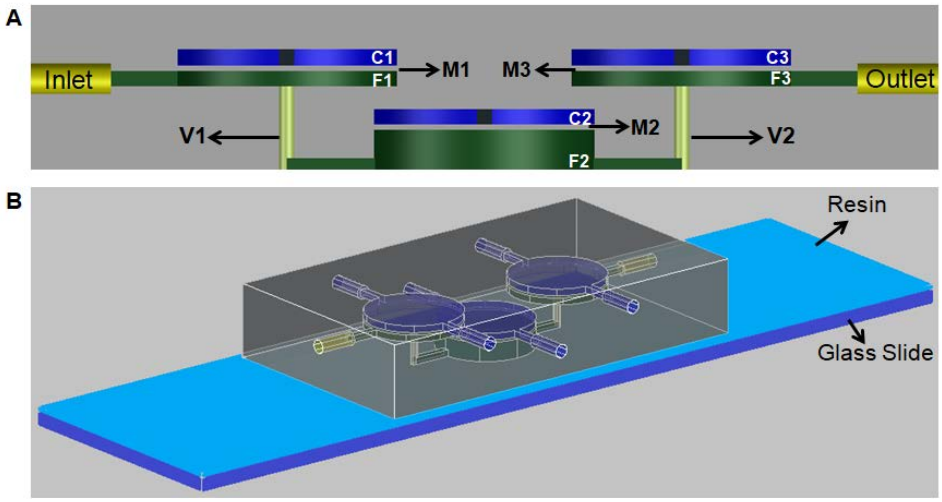

Figure 2.9. Design and fabrication of 3D-printed micropump. (A) Design of micropump having three control channels (C1, C2, C3), three fluidic channels (F1, F2, F3), three membranes (M1, M2, M3) and two via (V1, V2). (B) Bonding of micropump on glass slide using resin.

The designed micropump was fabricated with 3D printer. After the fabrication process, resin residue in the 3D-printed micropump was completely removed washing with isopropanol. Using direct bonding technique, 3D-printed micropump was bonded on 1000 rpm resin coated glass slide by applying of UV light for 10s (Figure 2.9.B).

2.2.4.3. Characterization of 3D-Printed Micropump

3D-printed micropump was actuated with air pressure. The membrane deformation of valves was controlled with peristaltic sequence having six phases using Arduino Uno microcontroller. The peristaltic sequence having configurations of 101, 100, 110, 010, 011 and 001 (0: open valve, 1: closed valve) was coded using Arduino software (Figure 2.10.). The Festo valves were integrated with Arduino setup and these valves were switched with 20 Hz frequency at 6.1 V_{DC}.

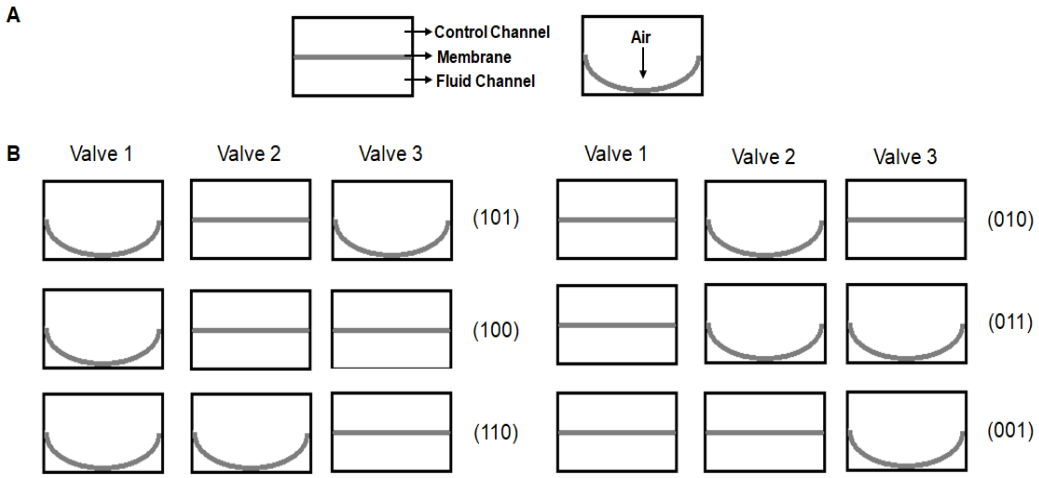

Figure 2.10. Illustration of peristaltic sequence. (A) Before and after applied air pressure, the motion of membrane. In the presence of air pressure, membrane deforms towards the bottom of fluid channel. (B) For each valve, peristaltic sequence situations and motion of membrane.

For characterization test, the outlets which locate at control channels of 3D-printed micropump was closed using epoxy and inlets of control channels was integrated with tubing of Festo valves. An ependorf tube filled with red food dye solution was connected to the inlet of fluidic channels using tubing and pump test was conducted by actuating membranes (Figure 2.11.).

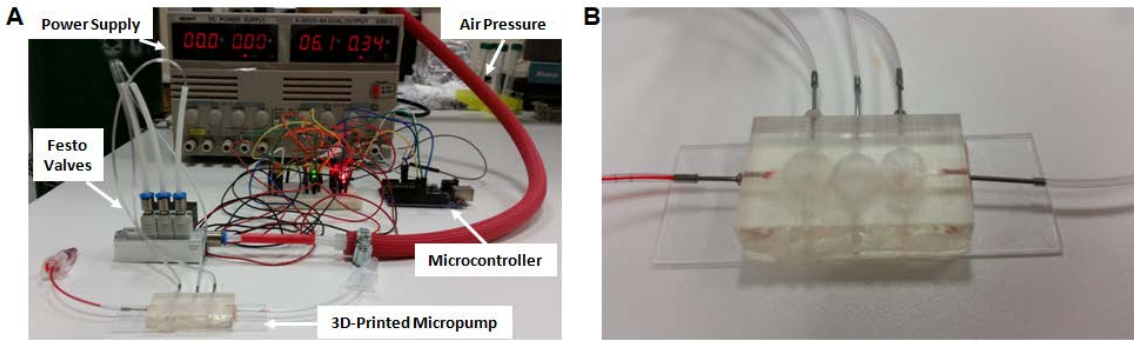

Figure 2.11. The characterization test setup of 3D-printed micropump. (A) Test setup that consists of a microcontroller, and pressure and power supply. (B) Top view of 3D-printed micropump.

CHAPTER 3

RESULTS AND DISCUSSION

3.1. Characterization and Performance Analysis of 3D Printer

The resolution of SLA 3D printer was analyzed using channels and molds having different shape and dimensions. After the fabrication process, height and width values of 3D-printed channels and molds were compared with designed ones using ImageJ software. Diameter and radius of semi-circular open channels are determined as their width and height dimensions, respectively. The cross-sectional illustrations of used channels and molds in image analyzing were given in Figure 3.3.

The semi-circular and rectangular open channels having 50 µm × 25 µm and 100 µm × 50 µm dimensions (width: height) were not printed successfully (Figure 3.1.A-C). Their molds with 50 µm × 25 µm (width: height) were also not printed (Figure 3.1.B-D).

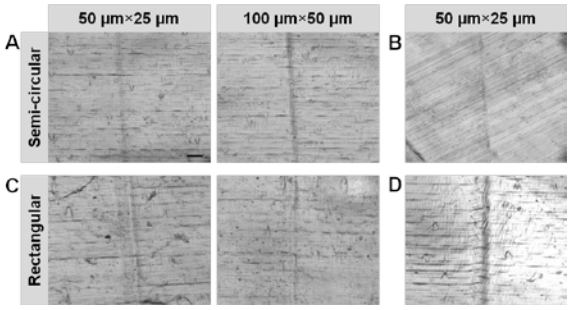

Figure 3.1. Micrographs of non-printed channels and molds dimensions. (A) Semi-circular open channels and (B) semi-circular mold. (C) Rectangular open channels and (D) rectangular mold. Scale bar is 200 µm.

In Figure 3.2., micrographs of fabricated channels and molds were given. According to image analysis, for semi-circular open channels, rectangular open channels and their molds having 2:1 aspect ratio (width: height), the difference between designed and fabricated width/height dimensions was gradually reduced when measurements of designed width and height were increased. For instance, a semi-circular open channel that has 150 µm × 75 µm designed dimensions resulted in 25 µm × 176.6 µm at the end of fabrication. However, when the semi-circular open channel was designed 500 µm × 250 µm, resulted dimensions of the channel are 408.4 µm × 261 µm. Although closed square channels have the same width and height dimensions, different results were obtained for width and height. For example, designed closed channel having 600 µm × 600 µm resulted in 670.6 µm × 925.7 µm cross-sectional dimensions. Consequently, it was determined that Formlabs Form 2 Desktop SLA 3D printer has different X/Y/Z resolution performance.

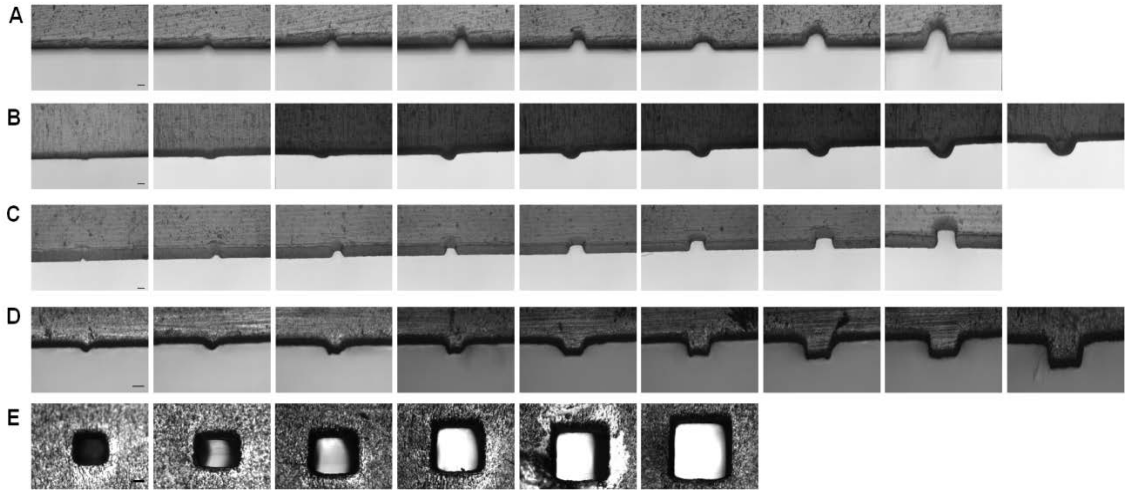

Figure 3.2. Micrographs of 3D-printed channels and correspondingly molds. (A) The semi-circular open channel, (B) semi-circular mold, (C) rectangular open channel, (D) rectangular mold. The designed height dimensions of semi-circular and rectangular open channels are 75 µm, 100 µm, 125 µm, 150 µm, 175 µm, 200 µm, 225 µm and 250 µm, respectively. The heights of molds are 50 µm, 75 µm, 100 µm, 125 µm, 150 µm, 175 µm, 200 µm, 225 µm and 250 µm, respectively. (E) The closed square channel having 500 µm, 600 µm, 700 µm, 800 µm, 900 µm and 1000 µm design dimensions, respectively. Scale bars are 200 µm.

Linear correlation between designed and fabricated dimensions was shown (Figure 3.3.). For designed semi-circular and rectangular open channels, at least 150 µm × 75 µm cross-sectional dimensions were printed and for their molds, at least 100 µm × 50 µm were also printed, successfully. These results show that fabricated width dimensions of semi-circular and rectangular channels have 66, 67% and 68% reduction, respectively. However, 17, 33% and 6, 67% increase were seen at fabricated height dimensions for semi-circular and rectangular channels, respectively. In addition to this, although rectangular molds have increasing dimensions at both fabricated width (12%) and height (169%), 54% decrease and 118% raise was seen at semi-circular fabricated width and height, respectively. Closed square channels having 500 µm × 500 µm cross-sectional dimensions were printed but inside of channels were clogged with resin during the printing process.

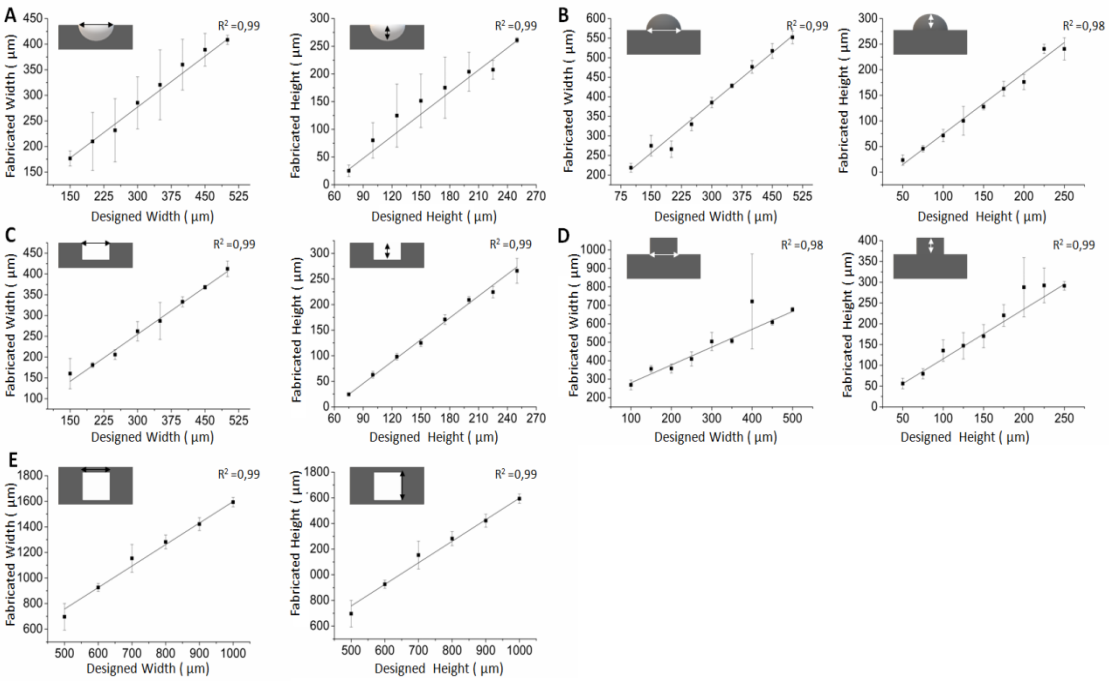

Figure 3.3. Correlation between designed and fabricated channels and molds dimensions for (A) semi-circular opened channel, (B) semi-circular mold, (C) rectangular opened channel, (D) rectangular mold and (F) closed square channel.

3.2. Characterization of Fabricated 3D-Printed Structures

3.2.1. Surface Angle Measurement

3D printer clear resin is composed of methacrylic acid esters and photoinitiator. For this reason, 3D-printed structures have a hydrophobic characteristic. However, these structures can be gained hydrophilic property treating with O_2 plasma. For instance, before O_2 plasma treatment, the surface contact angle of 3D-printed structures, glass and PDMS substrates was 97.5°, 15.9° and 105.7°, respectively (Figure 3.4.A-C.). Nevertheless, after O_2 plasma treatment, the surface contact angle of 3D-printed structures, glass and PDMS structures was reduced to 29.7 °, 6.3° and 4.5 °, respectively (Figure 3.4.B-D). Therefore, it was shown that 3D-printed structures using Formlabs Clear Resin can be easily used in microfluidic applications.

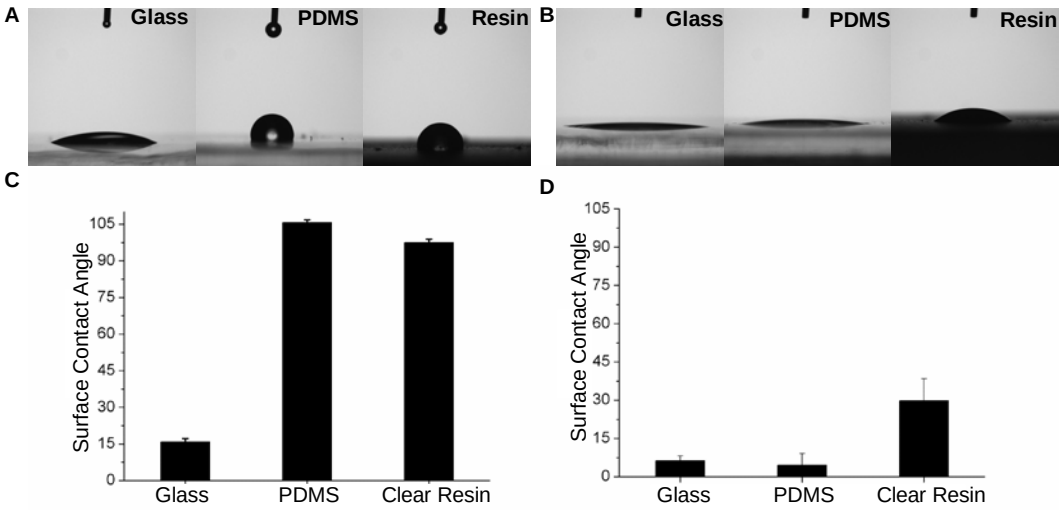

Figure 3.4. Surface contact angle measurements. Before and after O_2 plasma treatment, (A) and (B) are images each substrate, respectively. (C) and (D) graphics for surface contact angle of substrates before and after O_2 plasma treatment, respectively.

3.2.2. Thickness Values of PDMS and Printer Clear Resin

10:1 ratio of PDMS and resin were coated on cleaned glass slides at different spinning speed (rpm) and coating process resulted in various PDMS and resin thickness values. Before and after the coating process, thicknesses of each glass slides and coated glass slides with PDMS and resin were measured using callipers. In prepared samples with PDMS, resulted thickness values were calculated as 107.3 µm, 49.6 µm, 20.3 µm and 10 µm for 1000 rpm, 2000 rpm, 3000 rpm and 4000 rpm, respectively (Figure 3.5.A). Thicknesses of resin were also 96.6 µm, 53.3 µm, 23.3 µm and 13.3 µm at 1000 rpm, 2000 rpm, 3000 rpm and 4000 rpm, respectively (Figure 3.5.B).

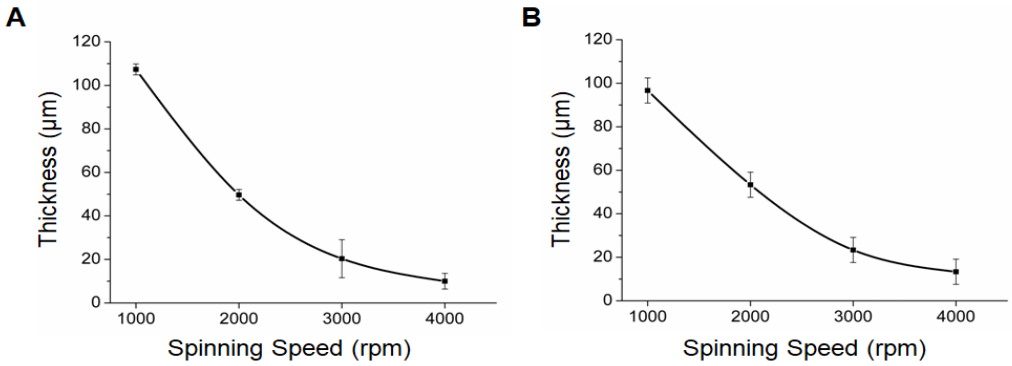

Figure 3.5. Coating thickness values. (A) PDMS and (B) resin thicknesses value at different spinning speed.

3.2.3. Accumulation of Printer Clear Resin on Glass Slide

The used resin tends to accumulation from the side of glass slide due to hydrophobic properties. Coated glass slide with resin at 1000 rpm was observed as time

depended. Use of resin just after coating process in presented bonding techniques was important in terms of attaining constant thickness values (Figure 3.6.).

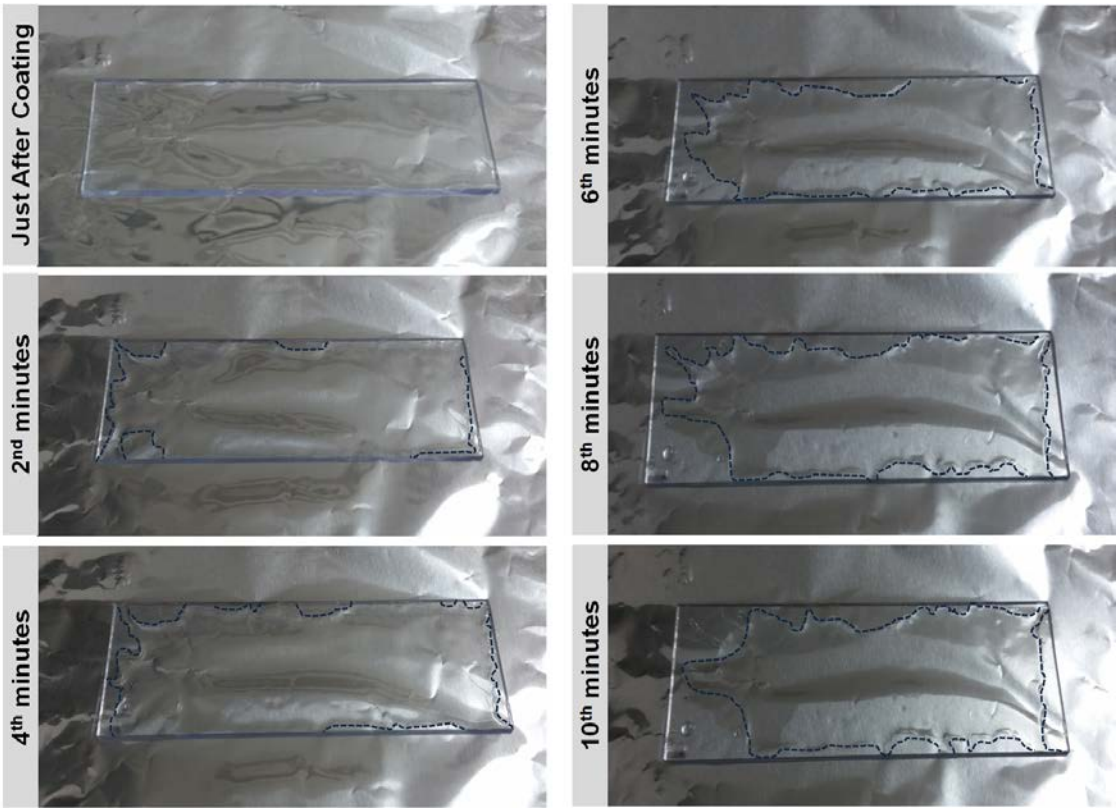

Figure 3.6. Time-depended resin accumulation. Images of coated glass slide were given after coated, and at 2nd min, 4thmin, 6th min, 8th min and 10th min.

3.2.4. Bonding Strength Test

Direct and transfer bonding techniques were used for fabrication of microfluidic chips by bonding of 3D-printed chambers to glass slides with PDMS and resin having different thickness values. The bonding strength of prepared microfluidic chips was

analyzed via applying air pressure and leakages from chips were monitored under microscope (Figure 3.7.).

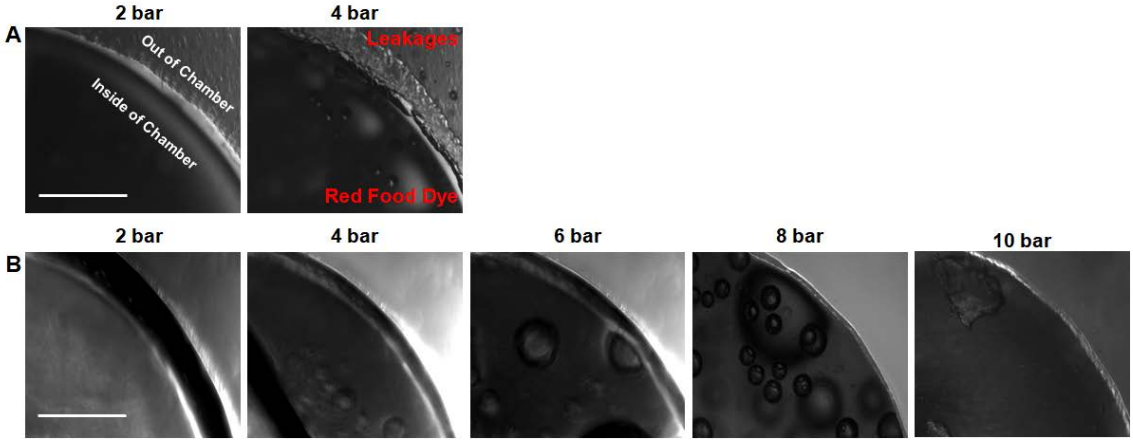

Figure 3.7. Micrographs of 3D-printed test chambers result during bonding strength test after applied pressure. (A) Prepared chamber using transfer bonding technique with 1000 rpm PDMS. The test chamber was resisted until 3.5 bar and leakages were shown at 4 bar. (B) Using transfer bonding technique, prepared chamber with 1000 rpm resin. The test chamber withstood up 10 bar. Scale bars are 200 µm.

The pressurized air pressure was applied to fabricated microfluidic chips with different PDMS and resin interlayer. The bonding strength was analyzed by monitoring leakages. In direct bonding technique using PDMS and resin at 1000 rpm, while prepared microfluidic chips with PDMS interlayer can resist until 8.8 bar, other chips with resin interlayer can endure down to 8.1 bar (Figure 3.8.A). At the same spinning speed, prepared chips using transfer bonding technique can withstand up to 3.6 bar and 8.6 bar for PDMS and resin interlayer, respectively (Figure 3.8.A). The bonding strength of prepared microfluidic chips with resin using transfer bonding technique is ~2-fold higher than bonding strength of traditional PDMS/glass bonding (4.5 bar) with oxygen plasma. At the result of the tensile stress test, a microfluidic chip which bonded on glass slide using transfer bonding technique can endure till 9.6 bar (Figure 3.8.B). Thickness values of PDMS and resin interlayer on glass slides affects bonding quality. For example, prepared chips with PDMS/resin interlayer using direct and transfer

bonding technique at 4000 rpm were not attached on glass slides. Although bonding strength is ~3.5 bar at 20 µm thickness for PDMS interlayer, thickness value <55µm resulted in maximum 1 bar bonding strength for resin interlayer. In the direct bonding technique, diminishing bonding strength associated with reducing thickness value was seen for PDMS interlayer, but sharp decreasing with low thickness value was shown for resin interlayer. For both PDMS and resin, low thickness value resulted in low bonding quality at transfer bonding technique.

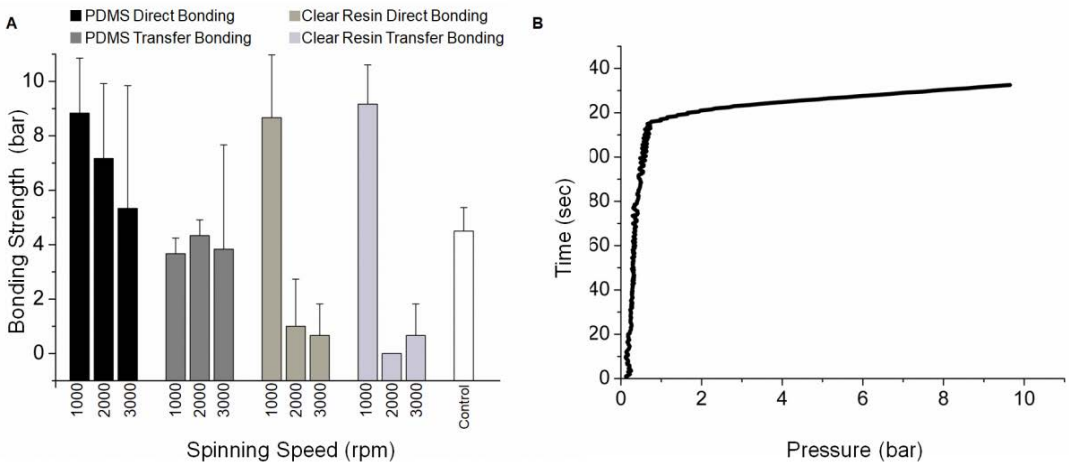

Figure 3.8. The results for bonding strength and tensile test. (A) Bonding strength results based on different thickness value of PDMS and resin interlayer. (B) Tensile stress test result for the prepared channel using transfer bonding technique with resin at 1000 rpm.

3.2.5. Surface Profile Analysis

The effect of bonding techniques to resulting channels heights was evaluated. For this purpose, 400 µm × 400 µm square open-ended channels were bonded on glass slides using presented bonding techniques at different spinning speeds. To analyze of channel heights, red food dye was injected to microfluidic channels. The prepared

channels with PDMS interlayer using both direct and transfer bonding techniques at 1000 rpm and 2000 rpm were clogging during the bonding process (Figure 3.9.A-B). However, only in direct bonding technique, prepared channels with resin at 1000 rpm were clogging (Figure 3.9.C.).

Channels fabricated with PDMS at 3000 rpm using direct and transfer bonding technique are completely functional. When fabricated channels using PDMS interlayer were compared with 3D-printed open-ended channels heights, it was shown that increasing at ratio of 1.27% and 5.7% in direct and transfer bonding techniques, respectively. Using resin, fully functional channels were fabricated at 1000 rpm and 2000 rpm for transfer and direct bonding technique, respectively. In direct and transfer bonding techniques, difference of height between fabricated channels and 3D-printed open-ended channels is 0.48% for resin interlayer (Figure 3.9.D.).

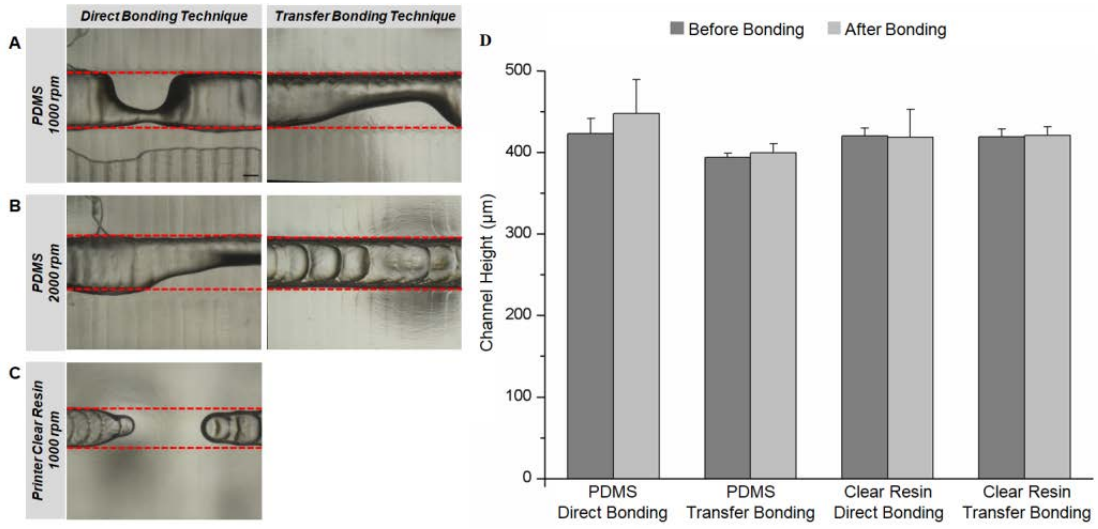

Figure 3.9. Images of clogging channels during bonding process with (A) and (B) PDMS and (C) resin interlayers. Scale bar is 200 µm. (D) Comparison of microfluidic channels height before and after the bonding process.

Moreover, 3D printed channels having 100 µm × 100 µm, 150 µm × 150 µm, 200 µm × 200 µm and 250 µm × 250 µm cross-sectional dimensions were bonded on

resin coated glass slides at 1000 rpm using transfer bonding technique. While fabricated channels having 100 µm × 100 µm, 150 µm × 150 µm and 200 µm × 200 µm dimensions were clogging after bonding process (Figure 3.10.), one of the three channels having 250 µm × 250 µm cross-sections was not clogging.

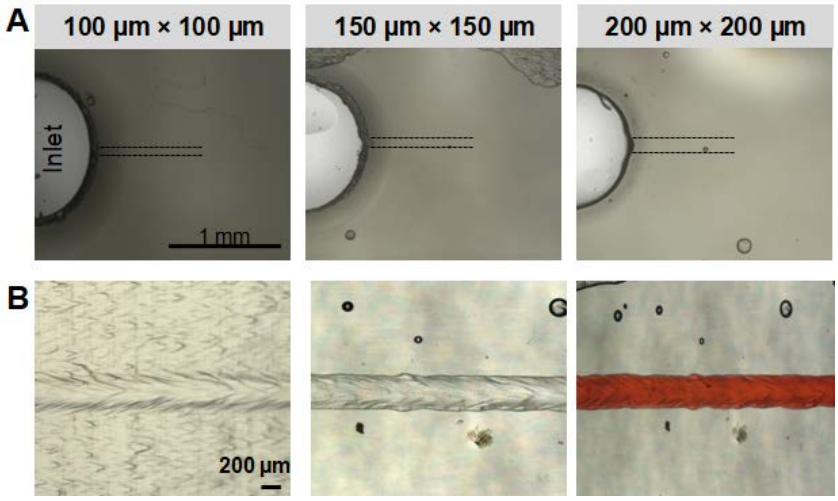

Figure 3.10. Micrographs for 3D-printed microchannels after the bonding process. (A) Micrographs of clogged channels for 100 µm × 100 µm, 150 µm × 150 µm and 200 µm × 200 µm cross-section, respectively. (B) Micrographs of before and after bonding process and red food dye-filled channel having 250 µm × 250 µm, respectively.

3.2.6. Microscopy Imaging of Fabricated Microfluidic Channels

In order to test optical transparency of fabricated channels, red food dye and fluorescent microsphere solution were injected to channels having 400 µm × 400 µm dimensions. Besides, for comparison, PDMS/glass chip with channel having 400 µm × 400 µm cross-section and completely 3D-printed closed square channel with 600 µm × 600 µm were fabricated. Wall thickness of 3D-printed closed square channel that same with glass slide thickness were designed as 1 mm. Red food dye was shown

with the naked eye at fabricated channels using direct and transfer bonding techniques (Figure 3.11.A). However, red food dye and fluorescent microspheres were not seen at a completely 3D-printed closed square channel (Figure 3.11.B.).

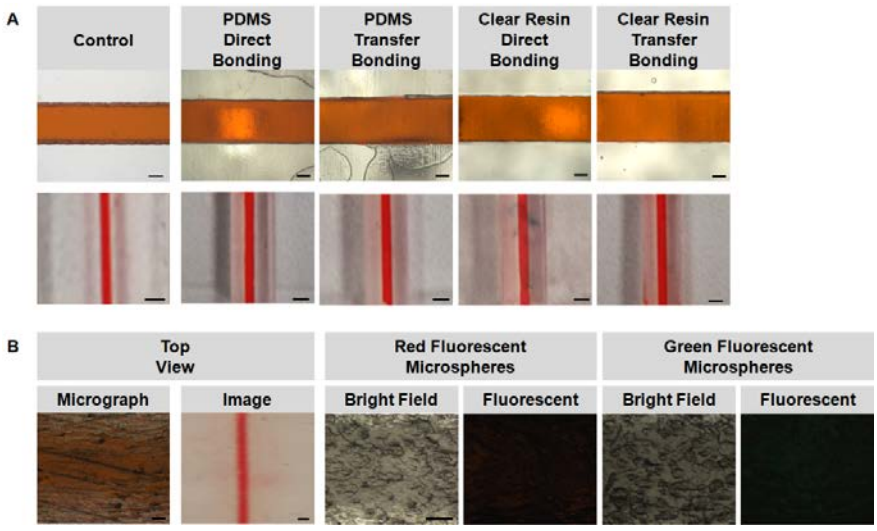

Figure 3.11. Micrographs and top view of fabricated channels. (A) Top view and images of prepared channels using different bonding technique. Scale bars are 200 µm. (B) Micrographs and top view of the 3D-printed closed channel with red food dye and bright field and fluorescent images of fluorescent microspheres. Scale bars are 200 µm for top view images of the 3D-printed closed square channel. For bright field and fluorescent images, scale bar is 50 µm.

Presented bonding techniques were allowed for bright-field and fluorescent imaging (Figure 3.12.A-B). Fluorescence intensity of red and green microspheres was evaluated and it was analyzed using one-way ANOVA combined with Newman-Keuls multiple comparisons test in all prepared channels. For red fluorescence intensity, statistically difference (p-value < 0.0001) was seen between the control group and other groups (Figure 3.12.C.). The green fluorescence intensity of fabricated channels with PDMS interlayer using direct bonding technique statistically differed (p-value < 0.05) from prepared channels with PDMS and resin interlayer using transfer bonding technique. However, the difference was not between the control group and other groups

(Figure 3.12.D). The red fluorescent intensity of fabricated channels is 1.35-1.5 fold lower than the control group. However, this difference in red fluorescent intensity resulted from background autofluorescence issues [89]. As a result, the fabricated channels using direct and transfer bonding techniques enable fluorescence imaging like traditional PDMS/glass chip.

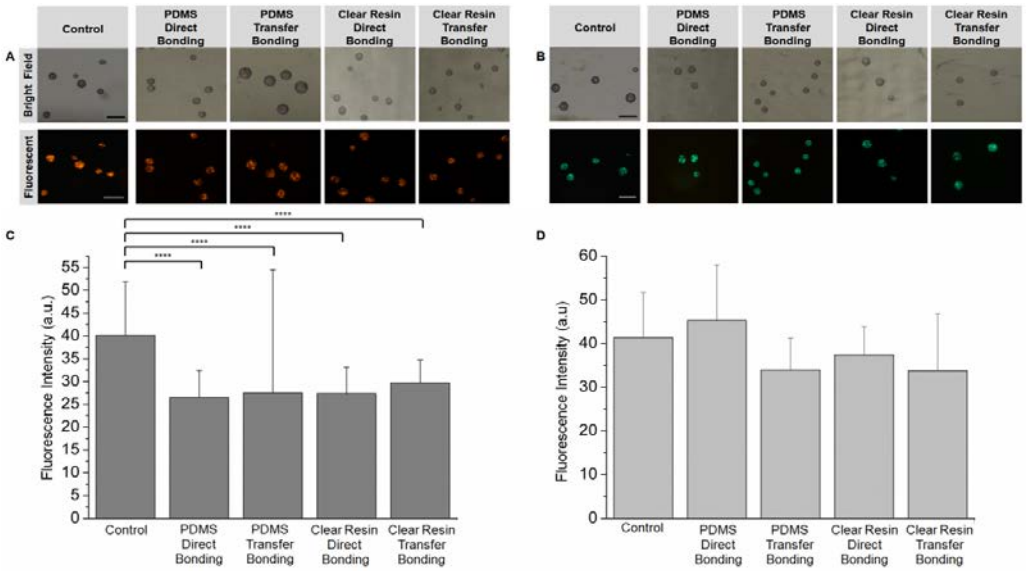

Figure 3.12. Analysis of fluorescence intensity. (A) red and (B) green fluorescent microspheres are bright-field and fluorescent images. Scale bars are 50 µm. Fluorescence intensity values of (C) red and (D) green microspheres. (****) indicates p-value < 0.0001.

3.3. Analysis of Protein Immobilization

Fabricated channels with resin at 1000 rpm using transfer bonding technique ensures fast processing time (30 s for spin coating and 10 s for UV exposure), superior bonding strength value (>9 bar), small channel dimensions (≥ 250 µm) and channel transparency for bright-field and fluorescence microscopy. Furthermore, microfluidic

chips can be bonded on glass surfaces having protein patterns using this bonding strategy and these fabrications can enhance the functionality of these microfluidic chips allowing many different biosensing applications including multiplex biomarker analysis.

The effect of transfer bonding technique to performance of Protein-G patterned on glass slides that labeled with fluorescence-tagged IgG (H+L) antibody inside fabricated channels was evaluated (Figure 3.13.A.). Statistically difference of fluorescence intensity was not seen between PDMS chip and 3D-printed chip which fabricated with transfer bonding technique using resin coated glass slide at 1000 rpm (p-value>0.05) (Figure 3.13.B.). BSA pattern and Protein-G pattern that is without fluorescent antibodies were compared with Protein-G pattern and they showed lower fluorescence intensity (p-value <0.001) (Figure 3.13.B.). According to these results, IgG antibodies are highly specific to Protein-G. Hence, presented bonding technique enables easily to integration of protein patterning inside microfluidic channels without altering the functionality of the protein.

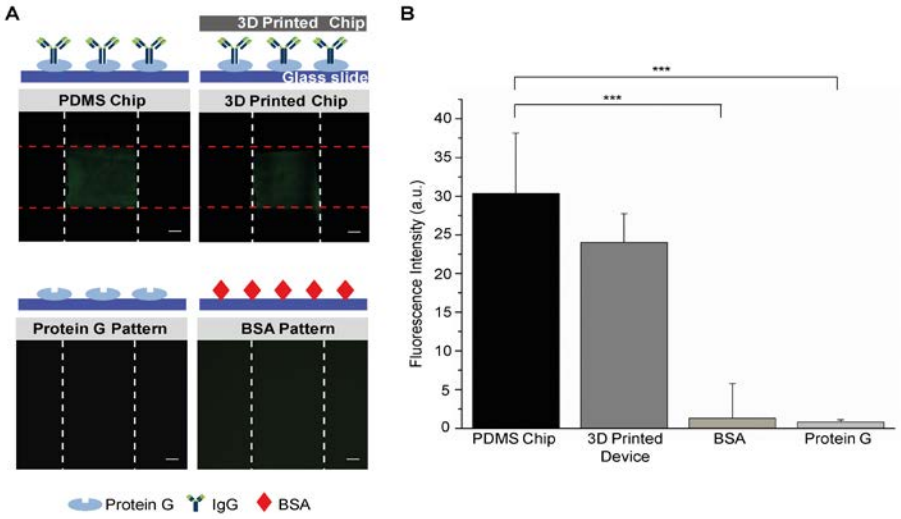

Figure 3.13. Analysis of Protein-G immobilization (A) Illustration and fluorescent micrographs. Scale bars are 200 µm. (B) Fluorescence intensity values for PDMS chip, 3D-printed chip, Protein-G and BSA pattern. Statistically, the difference was evaluated with one-way ANOVA combined with Newman-Keuls multiple comparisons test.

3.4. Characterization of Membrane Deformation

Using Eq.3, predicted membrane deformation pressure for first (t = 250 µm, y = 250 µm and r = 5000 µm) and second model (t = 500 µm, y = 250 µm and r = 5000 µm) was calculated as 1.85 bar and 2.05 bar, respectively. The air pressure was applied to 3D-printed devices at intervals of 2 min. For the first 3D-printed device, when 2 bar and 4 bar pressure were applied, heights of membrane deformation were 1345.14 µm and 1378.98 µm, respectively. However, the membrane of the first 3D-printed device was completely burst at 6 bar pressure. The membrane deformation heights of the second 3D-printed device were also 67.68 µm, 287.64 µm and 423 µm at 2 bar, 4 bar and 6 bar, respectively and the membrane of this device was also burst at 8 bar pressure. Although analyzed deformation height of membrane was 5-fold higher than calculated value using Eq.3 in the first 3D-printed device at 2 bar. The deformation height of second 3D-printed device was also lower 3.7-fold than predicting height at the same pressure value.

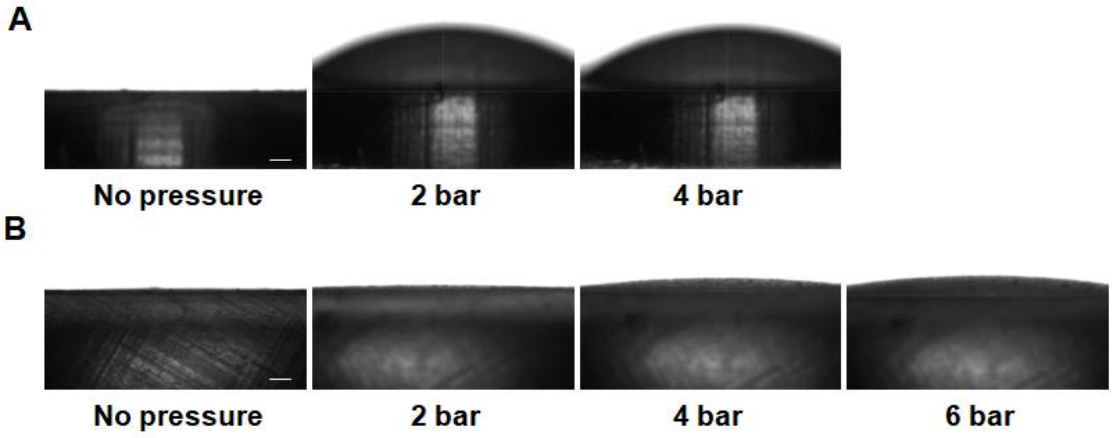

Figure 3.14. Micrographs for 3D-printed membrane deformation devices before and after applied pressure. (A) First 3D-printed device and (B) Second 3D-printed device. Scale bars are 500 µm.

CHAPTER 4

CONCLUSION

The aims of this thesis are rapidly fabrication of microfluidic devices via 3D printer and enhance optically transparency of 3D-printed devices. The all 3D models were designed by AutoCAD program and they fabricated with Formlabs Form 2 Desktop SLA 3D printer at short time (< 6 hr). According to performance analysis of 3D printer, microfluidic channels having 25 µm fabrication dimensions were printed, successfully. In closed square channels, channel dimensions equal and larger than 600 µm were successfully fabricated without any channel-clogging problem. However, 3D-printed closed square channels have not optical transparency and for this reason, they were not suitable for microscopic imaging.

Using presented bonding techniques, channels having down 250 µm dimensions were bonded and these techniques enable fabrication of optically transparent 3D-printed microfluidic channels. Different bonding strength values were obtained for PDMS and resin interlayer at various coating thickness and bonding strength was obtained up to 2-fold higher than traditional bonded PDMS/glass chip with plasma treatment (4.5 bar). For prepared 3D-printed devices using resin, bonding strength value was 2.5-fold higher than 3D-printed devices with PDMS for both direct and transfer bonding techniques.

Furthermore, presented bonding techniques allow bright-field and fluorescent microscopy imaging due to the optically transparent property of PDMS and resin. 3D-printed channels prepared using presented bonding techniques can be observed with naked eye or microscope. The fluorescence intensity analysis of red and green microspheres shown that the presented bonding techniques are suitable for fluorescent imaging application. Moreover, the presented bonding techniques can slight change the heights of 3D-printed channels. However, the height difference was only 5.8% at the most. Although bonding techniques with PDMS interlayer require higher processing

time than 12 hr for fabrication and curing, bonding techniques with resin interlayer provide a short processing time (<1 min; spin coating for 30 s and curing with UV light for 10 s). Moreover, 3D-printed microfluidic channels were easily bonded on protein modified glass slides at short time using transfer bonding technique with resin.

For membrane actuated 3D-printed micropump, membrane deformation values were calculated with two deformation models, theoretically. The results of test applying pressurized air to 3D-printed deformation devices shown that theoric membrane deformation heights differed from heights which are occurred after applying pressure.

In the future perspective, fabrication of microfluidic devices with 3D printer can provide rapid prototyping for microfluidic applications. The presented bonding techniques enhance optical imaging properties of 3D-printed microfluidic devices and these techniques enable new functionality with integrating of patterned biological molecules. For these reasons, these bonding techniques can be disseminated usage of 3D-printed microfluidic devices in the field of biomedical, especially biosensing applications. The proposed membrane actuated micropump integrated to 3D-printed microfluidic devices can be used to drive fluid in microfluidic channels for automated operation of various applications.

REFERENCES

1. Lee, J. M.; Zhang, M.; Yeong, W. Y., Characterization and evaluation of 3D printed microfluidic chip for cell processing. *Microfluidics and Nanofluidics*, **2016,** *20* (1), 5.

2. McDonald, J. C.; Whitesides, G. M., Poly (dimethylsiloxane) as a material for fabricating microfluidic devices. *Accounts of chemical research* **2002,** *35* (7), 491-499.

3. Ho, C. M. B.; Ng, S. H.; Li, K. H. H.; Yoon, Y.-J., 3D printed microfluidics for biological applications. *Lab on a Chip* **2015,** *15* (18), 3627-3637.

4. Ren, K.; Zhou, J.; Wu, H., Materials for microfluidic chip fabrication. *Accounts of chemical research* **2013,** *46* (11), 2396-2406.

5. O'Neill, P. F.; Ben Azouz, A.; Vazquez, M.; Liu, J.; Marczak, S.; Slouka, Z.; Chang, H. C.; Diamond, D.; Brabazon, D., Advances in three-dimensional rapid prototyping of microfluidic devices for biological applications. *Biomicrofluidics* **2014,** *8* (5), 052112.

6. Saggiomo, V.; Velders, A. H., Simple 3D printed scaffold-removal method for the fabrication of intricate microfluidic devices. *Advanced Science* **2015,** *2* (9), 1500125.

7. Rogers, C. I.; Qaderi, K.; Woolley, A. T.; Nordin, G. P., 3D printed microfluidic devices with integrated valves. *Biomicrofluidics* **2015,** *9* (1), 016501.

8. Grover, W. H.; Skelley, A. M.; Liu, C. N.; Lagally, E. T.; Mathies, R. A., Monolithic membrane valves and diaphragm pumps for practical large-scale integration into glass microfluidic devices. *Sensors and Actuators B: Chemical* **2003,** *89* (3), 315-323.

9. Sahore, V.; Kumar, S.; Rogers, C.; Jensen, J.; Sonker, M.; Woolley, A., Pressure-actuated microfluidic devices for electrophoretic separation of pre-term birth biomarkers. *Analytical and bioanalytical chemistry* **2016,** *408* (2), 599-607.

10. Lau, A.; Yip, H.; Ng, K.; Cui, X.; Lam, R., Dynamics of microvalve operations in integrated microfluidics. *Micromachines* **2014,** *5* (1), 50-65.

11. Cai, Z.; Xiang, J.; Chen, H.; Wang, W., Membrane-based valves and inward-pumping system for centrifugal microfluidic platforms. *Sensors and Actuators B: Chemical* **2016,** *228*, 251-258.

12. Abate, A.; Weitz, D., Single-layer membrane valves for elastomeric microfluidic devices. *Applied Physics Letters* **2008,** *92* (24), 243509.

13. Au, A. K.; Lai, H.; Utela, B. R.; Folch, A., Microvalves and micropumps for BioMEMS. *Micromachines* **2011,** *2* (2), 179-220.

14. Nge, P. N.; Rogers, C. I.; Woolley, A. T., Advances in microfluidic materials, functions, integration, and applications. *Chemical reviews* **2013,** *113* (4), 2550-2583.

15. Thio, T. H. G.; Soroori, S.; Ibrahim, F.; Al-Faqheri, W.; Soin, N.; Kulinsky, L.; Madou, M., Theoretical development and critical analysis of burst frequency equations for passive valves on centrifugal microfluidic platforms. *Medical & biological engineering & computing* **2013,** *51* (5), 525-535.

16. Cho, H.; Kim, H.-Y.; Kang, J. Y.; Kim, T. S., How the capillary burst microvalve works. *Journal of colloid and interface science* **2007,** *306* (2), 379-385.

17. Kim, J.; Stockton, A. M.; Jensen, E. C.; Mathies, R. A., Pneumatically actuated microvalve circuits for programmable automation of chemical and biochemical analysis. *Lab on a Chip* **2016,** *16* (5), 812-819.

18. Kim, J. H.; Lau, K. T.; Shepherd, R.; Wu, Y.; Wallace, G.; Diamond, D., Performance characteristics of a polypyrrole modified polydimethylsiloxane (PDMS) membrane based microfluidic pump. *Sensors and Actuators A: Physical* **2008,** *148* (1), 239-244.

19. Unger, M. A.; Chou, H.-P.; Thorsen, T.; Scherer, A.; Quake, S. R., Monolithic microfabricated valves and pumps by multilayer soft lithography. *Science* **2000,** *288* (5463), 113-116.

20. Yang, Y.-N.; Hsiung, S.-K.; Lee, G.-B., A pneumatic micropump incorporated with a normally closed valve capable of generating a high pumping rate and a high back pressure. *Microfluidics and Nanofluidics* **2008,** *6* (6), 823-833.

21. Hosokawa, K.; Maeda, R., A pneumatically-actuated three-way microvalve fabricated with polydimethylsiloxane using the membrane transfer technique. *Journal of micromechanics and microengineering* **2000,** *10* (3), 415.

22. Kim, J.; Kang, M.; Jensen, E. C.; Mathies, R. A., Lifting gate polydimethylsiloxane microvalves and pumps for microfluidic control. *Analytical chemistry* **2012,** *84* (4), 2067-2071.

23. Ke, M.-T.; Zhong, J.-H.; Lee, C.-Y., Electromagnetically-actuated reciprocating pump for high-flow-rate microfluidic applications. *Sensors* **2012,** *12* (10), 13075-13087.

24. Thomas, D.; Tehrani, Z.; Redfearn, B., 3-D printed composite microfluidic pump for wearable biomedical applications. *Additive Manufacturing* **2016,** *9*, 30-38.

25. Taylor, A. P.; Velásquez-García, L. F. In *3-D printed miniaturized diaphragm vacuum pump*, 2017 IEEE 30th International Conference on Micro Electro Mechanical Systems (MEMS), IEEE: 2017; pp 1292-1295.

26. Nguyen, N.-T.; Huang, X.; Chuan, T. K., MEMS-micropumps: a review. *Journal of fluids Engineering* **2002,** *124* (2), 384-392.

27. Nisar, A.; Afzulpurkar, N.; Mahaisavariya, B.; Tuantranont, A., MEMS-based micropumps in drug delivery and biomedical applications. *Sensors and Actuators B: Chemical* **2008,** *130* (2), 917-942.

28. Feng, G.-H.; Kim, E. S., Piezoelectrically actuated dome-shaped diaphragm micropump. *Journal of microelectromechanical systems* **2005,** *14* (2), 192-199.

29. Xiang, J.; Cai, Z.; Zhang, Y.; Wang, W., A micro-cam actuated linear peristaltic pump for microfluidic applications. *Sensors and Actuators A: Physical* **2016,** *251*, 20-25.

30. Tseng, H.-Y.; Wang, C.-H.; Lin, W.-Y.; Lee, G.-B., Membrane-activated microfluidic rotary devices for pumping and mixing. *Biomedical microdevices* **2007,** *9* (4), 545-554.

31. Anderson, K. B.; Lockwood, S. Y.; Martin, R. S.; Spence, D. M., A 3D printed fluidic device that enables integrated features. *Analytical chemistry* **2013,** *85* (12), 5622-5626.

32. Au, A. K.; Bhattacharjee, N.; Horowitz, L. F.; Chang, T. C.; Folch, A., 3D-printed microfluidic automation. *Lab on a chip* **2015,** *15* (8), 1934-1941.

33. Bhattacharjee, N.; Parra-Cabrera, C.; Kim, Y. T.; Kuo, A. P.; Folch, A., Desktop-Stereolithography 3D - Printing of a Poly (dimethylsiloxane)- Based Material with Sylgard-184 Properties. *Advanced Materials* **2018,** *30* (22), 1800001.

34. Peng, L.; Deng, Y.; Yi, P.; Lai, X., Micro hot embossing of thermoplastic polymers: a review. *Journal of Micromechanics and Microengineering* **2013,** *24* (1), 013001.

35. Ziaie, B.; Baldi, A.; Lei, M.; Gu, Y.; Siegel, R. A., Hard and soft micromachining for BioMEMS: review of techniques and examples of applications in microfluidics and drug delivery. *Advanced drug delivery reviews* **2004,** *56* (2), 145-172.

36. Verpoorte, E.; De Rooij, N. F., Microfluidics meets MEMS. *Proceedings of the IEEE* **2003,** *91* (6), 930-953.

37. Xia, Y.; Whitesides, G. M., Soft lithography. *Angewandte Chemie International Edition* **1998,** *37* (5), 550-575.

38. Xia, Y.; Rogers, J. A.; Paul, K. E.; Whitesides, G. M., Unconventional methods for fabricating and patterning nanostructures. *Chemical reviews* **1999,** *99* (7), 1823-1848.

39. Tan, H. Y.; Loke, W. K.; Nguyen, N.-T., A reliable method for bonding polydimethylsiloxane (PDMS) to polymethylmethacrylate (PMMA) and its application in micropumps. *Sensors and Actuators B: Chemical* **2010,** *151* (1), 133-139.

40. Jothimuthu, P.; Carroll, A.; Bhagat, A. A. S.; Lin, G.; Mark, J. E.; Papautsky, I., Photodefinable PDMS thin films for microfabrication applications. *Journal of Micromechanics and Microengineering* **2009,** *19* (4).

41. Hwang, Y.; Paydar, O. H.; Candler, R. N., 3D printed molds for non-planar PDMS microfluidic channels. *Sensors and Actuators A: Physical* **2015,** *226*, 137-142.

42. Au, A. K.; Lee, W.; Folch, A., Mail-order microfluidics: evaluation of stereolithography for the production of microfluidic devices. *Lab on a Chip* **2014,** *14* (7), 1294-1301.

43. Gross, B. C.; Erkal, J. L.; Lockwood, S. Y.; Chen, C.; Spence, D. M., Evaluation of 3D printing and its potential impact on biotechnology and the chemical sciences. ACS Publications: 2014.

44. Sochol, R.; Sweet, E.; Glick, C.; Venkatesh, S.; Avetisyan, A.; Ekman, K.; Raulinaitis, A.; Tsai, A.; Wienkers, A.; Korner, K., 3D printed microfluidic circuitry via multijet-based additive manufacturing. *Lab on a Chip* **2016,** *16* (4), 668-678.

45. Shallan, A. I.; Smejkal, P.; Corban, M.; Guijt, R. M.; Breadmore, M. C., Cost-effective three-dimensional printing of visibly transparent microchips within minutes. *Analytical chemistry* **2014,** *86* (6), 3124-3130.

46. Amin, R.; Knowlton, S.; Hart, A.; Yenilmez, B.; Ghaderinezhad, F.; Katebifar, S.; Messina, M.; Khademhosseini, A.; Tasoglu, S., 3D-printed microfluidic devices. *Biofabrication* **2016,** *8* (2), 022001.

47. Zhang, Y.; Ge, S.; Yu, J., Chemical and biochemical analysis on lab-on-a-chip devices fabricated using three-dimensional printing. *TrAC Trends in Analytical Chemistry* **2016,** *85*, 166-180.

48. Yazdi, A. A.; Popma, A.; Wong, W.; Nguyen, T.; Pan, Y.; Xu, J., 3D printing: an emerging tool for novel microfluidics and lab-on-a-chip applications. *Microfluidics and Nanofluidics* **2016,** *20* (3), 50.

49. Stansbury, J. W.; Idacavage, M. J., 3D printing with polymers: Challenges among expanding options and opportunities. *Dent Mater* **2016,** *32* (1), 54-64.

50. Bhattacharjee, N.; Urrios, A.; Kang, S.; Folch, A., The upcoming 3D-printing revolution in microfluidics. *Lab on a Chip* **2016,** *16* (10), 1720-1742.

51. Ho, C. M.; Ng, S. H.; Li, K. H.; Yoon, Y. J., 3D printed microfluidics for biological applications. *Lab Chip* **2015,** *15* (18), 3627-37.

52. Au, A. K.; Huynh, W.; Horowitz, L. F.; Folch, A., 3D-Printed Microfluidics. *Angew Chem Int Ed Engl* **2016,** *55* (12), 3862-81.

53. Waheed, S.; Cabot, J. M.; Macdonald, N. P.; Lewis, T.; Guijt, R. M.; Paull, B.; Breadmore, M. C., 3D printed microfluidic devices: enablers and barriers. *Lab on a Chip* **2016,** *16* (11), 1993-2013.

54. Paydar, O. H.; Paredes, C. N.; Hwang, Y.; Paz, J.; Shah, N. B.; Candler, R. N., Characterization of 3D-printed microfluidic chip interconnects with integrated O-rings. *Sensors and Actuators A: Physical* **2014,** *205*, 199-203.

55. Kamei, K.; Mashimo, Y.; Koyama, Y.; Fockenberg, C.; Nakashima, M.; Nakajima, M.; Li, J.; Chen, Y., 3D printing of soft lithography mold for rapid production of polydimethylsiloxane-based microfluidic devices for cell stimulation with concentration gradients. *Biomed Microdevices* **2015,** *17* (2), 36.

56. McDonald, J. C.; Chabinyc, M. L.; Metallo, S. J.; Anderson, J. R.; Stroock, A. D.; Whitesides, G. M., Prototyping of microfluidic devices in poly (dimethylsiloxane) using solid-object printing. *Analytical chemistry* **2002,** *74* (7), 1537-1545.

57. Bonyár, A.; Sántha, H.; Ring, B.; Varga, M.; Gábor Kovács, J.; Harsányi, G., 3D Rapid Prototyping Technology (RPT) as a powerful tool in microfluidic development. *Procedia Engineering* **2010,** *5*, 291-294.

58. Comina, G.; Suska, A.; Filippini, D., PDMS lab-on-a-chip fabrication using 3D printed templates. *Lab on a Chip* **2014,** *14* (2), 424-430.

59. Chan, H. N.; Chen, Y.; Shu, Y.; Chen, Y.; Tian, Q.; Wu, H., Direct, one-step molding of 3D-printed structures for convenient fabrication of truly 3D PDMS microfluidic chips. *Microfluidics and nanofluidics* **2015,** *19* (1), 9-18.

60. Olanrewaju, A. O.; Robillard, A.; Dagher, M.; Juncker, D., Autonomous microfluidic capillaric circuits replicated from 3D-printed molds. *Lab Chip* **2016,** *16* (19), 3804-3814.

61. Kang, K.; Oh, S.; Yi, H.; Han, S.; Hwang, Y., Fabrication of truly 3D microfluidic channel using 3D-printed soluble mold. *Biomicrofluidics* **2018,** *12* (1), 014105.

62. Takenaga, S.; Schneider, B.; Erbay, E.; Biselli, M.; Schnitzler, T.; Schöning, M. J.; Wagner, T., Fabrication of biocompatible lab-on-chip devices for biomedical applications by means of a 3D-printing process. *physica status solidi (a)* **2015,** *212* (6), 1347-1352.

63. Ong, L. J. Y.; Islam, A.; DasGupta, R.; Iyer, N. G.; Leo, H. L.; Toh, Y.-C., A 3D printed microfluidic perfusion device for multicellular spheroid cultures. *Biofabrication* **2017,** *9* (4), 045005.

64. Lee, W.; Kwon, D.; Choi, W.; Jung, G. Y.; Jeon, S., 3D-printed microfluidic device for the detection of pathogenic bacteria using size-based separation in helical channel with trapezoid cross-section. *Sci Rep* **2015,** *5*, 7717.

65. Gong, H.; Woolley, A. T.; Nordin, G. P., High density 3D printed microfluidic valves, pumps, and multiplexers. *Lab on a Chip* **2016,** *16* (13), 2450-2458.

66. Lee, Y. S.; Bhattacharjee, N.; Folch, A., 3D-printed Quake-style microvalves and micropumps. *Lab Chip* **2018,** *18* (8), 1207-1214.

67. Chen, C.; Mehl, B. T.; Munshi, A. S.; Townsend, A. D.; Spence, D. M.; Martin, R. S., 3D-printed microfluidic devices: fabrication, advantages and limitations—a mini review. *Analytical Methods* **2016,** *8* (31), 6005-6012.

68. Lee, K. G.; Park, K. J.; Seok, S.; Shin, S.; Park, J. Y.; Heo, Y. S.; Lee, S. J.; Lee, T. J., 3D printed modules for integrated microfluidic devices. *Rsc Advances* **2014,** *4* (62), 32876-32880.

69. Gong, H.; Beauchamp, M.; Perry, S.; Woolley, A. T.; Nordin, G. P., Optical approach to resin formulation for 3D printed microfluidics. *RSC advances* **2015,** *5* (129), 106621-106632.

70. Macdonald, N. P.; Cabot, J. M.; Smejkal, P.; Guijt, R. M.; Paull, B.; Breadmore, M. C., Comparing microfluidic performance of three-dimensional (3D) printing platforms. *Analytical chemistry* **2017,** *89* (7), 3858-3866.

71. Romanov, V.; Samuel, R.; Chaharlang, M.; Jafek, A. R.; Frost, A.; Gale, B. K., FDM 3D Printing of High-Pressure, Heat-Resistant, Transparent Microfluidic Devices. *Analytical chemistry* **2018,** *90* (17), 10450-10456.

72. Gross, B. C.; Anderson, K. B.; Meisel, J. E.; McNitt, M. I.; Spence, D. M., Polymer coatings in 3D-printed fluidic device channels for improved cellular adherence prior to electrical lysis. *Analytical chemistry* **2015,** *87* (12), 6335-6341.

73. Zhu, F.; Skommer, J.; Macdonald, N. P.; Friedrich, T.; Kaslin, J.; Wlodkowic, D., Three-dimensional printed millifluidic devices for zebrafish embryo tests. *Biomicrofluidics* **2015,** *9* (4), 046502.

74. Kotz, F.; Risch, P.; Helmer, D.; Rapp, B. E., Highly Fluorinated Methacrylates for Optical 3D Printing of Microfluidic Devices. *Micromachines* **2018,** *9* (3), 115.

75. Urrios, A.; Parra-Cabrera, C.; Bhattacharjee, N.; Gonzalez-Suarez, A. M.; Rigat-Brugarolas, L. G.; Nallapatti, U.; Samitier, J.; DeForest, C. A.; Posas, F.; Garcia-Cordero, J. L.; Folch, A., 3D-printing of transparent bio-microfluidic devices in PEG-DA. *Lab Chip* **2016,** *16* (12), 2287-94.

76. Bressan, L. P.; Robles-Najar, J.; Adamo, C. B.; Quero, R. F.; Costa, B. M. C.; de Jesus, D. P.; da Silva, J. A. F., 3D-printed microfluidic device for the synthesis of silver and gold nanoparticles. *Microchemical Journal* **2019,** *146*, 1083-1089.

77. Yao, P.; Xu, T.; Tung, S. In *Pneumatic Microfluidic Device by 3D Printing Technology for Insulin Determination*, 2018 IEEE 12th International Conference on Nano/Molecular Medicine and Engineering (NANOMED), IEEE: 2018; pp 224-227.

78. Lynh, H. D.; Pin-Chuan, C., Novel solvent bonding method for creation of a three-dimensional, non-planar, hybrid PLA/PMMA microfluidic chip. *Sensors and Actuators A: Physical* **2018,** *280*, 350-358.

79. Zips, S.; Wenzel, O. J.; Rinklin, P.; Grob, L.; Terkan, K.; Adly, N. Y.; Weiß, L.; Wolfrum, B., Direct Stereolithographic 3D Printing of Microfluidic Structures on Polymer Substrates for Printed Electronics. *Advanced Materials Technologies* **2019,** *4* (3), 1800455.

80. Wilhelm, E.; Neumann, C.; Sachsenheimer, K.; Schmitt, T.; Länge, K.; Rapp, B. E., Rapid bonding of polydimethylsiloxane to stereolithographically manufactured epoxy components using a photogenerated intermediary layer. *Lab on a Chip* **2013,** *13* (12), 2268-2271.

81. Hamad, E.; Bilatto, S.; Adly, N.; Correa, D.; Wolfrum, B.; Schöning, M. J.; Offenhäusser, A.; Yakushenko, A., Inkjet printing of UV-curable adhesive and dielectric inks for microfluidic devices. *Lab on a Chip* **2016,** *16* (1), 70-74.

82. Kadimisetty, K.; Spak, A. P.; Bhalerao, K. S.; Sharafeldin, M.; Mosa, I. M.; Lee, N. H.; Rusling, J. F., Automated 4-Sample Protein Immunoassays using 3D-Printed Microfluidics. *Anal Methods* **2018,** *10* (32), 4000-4006.

83. Tekin, H. C.; Gijs, M. A., Ultrasensitive protein detection: a case for microfluidic magnetic bead-based assays. *Lab Chip* **2013,** *13* (24), 4711-39.

84. Tekin, H. C.; Cornaglia, M.; Gijs, M. A., Attomolar protein detection using a magnetic bead surface coverage assay. *Lab on a Chip* **2013,** *13* (6), 1053-1059.

85. Kadimisetty, K.; Malla, S.; Bhalerao, K. S.; Mosa, I. M.; Bhakta, S.; Lee, N. H.; Rusling, J. F., Automated 3D-Printed Microfluidic Array for Rapid Nanomaterial-Enhanced Detection of Multiple Proteins. *Anal Chem* **2018,** *90* (12), 7569-7577.

86. Lepowsky, E.; Amin, R.; Tasoglu, S., Assessing the Reusability of 3D-Printed Photopolymer Microfluidic Chips for Urine Processing. *Micromachines (Basel)* **2018,** *9* (10).

87. Tang, C. K.; Vaze, A.; Rusling, J. F., Automated 3D-printed unibody immunoarray for chemiluminescence detection of cancer biomarker proteins. *Lab Chip* **2017,** *17* (3), 484-489.

88. Bressan, L. P.; Adamo, C. B.; Quero, R. F.; de Jesus, D. P.; da Silva, J. A. F., A simple procedure to produce FDM-based 3D-printed microfluidic devices with an integrated PMMA optical window. *Analytical Methods* **2019,** *11* (8), 1014-1020.

89. Salentijn, G. I.; Oomen, P. E.; Grajewski, M.; Verpoorte, E., Fused deposition modeling 3D printing for (bio) analytical device fabrication: procedures, materials, and applications. *Analytical chemistry* **2017,** *89* (13), 7053-7061.